Enhanced sulfur in the UTLS in spring 2020

Laura Tomsche[1,2], Andreas Marsing[1,2], Tina Jurkat-Witschas[1], Johannes Lucke[1,5], Stefan Kaufmann[1], Katharina Kaiser[3], Johannes Schneider[3], Monika Scheibe[1], Hans Schlager[1], Lenard Röder[3], Horst Fischer[3], Florian Obersteiner[4], Andreas Zahn[4], Martin Zöger[6], Jos Lelieveld[3], Christiane Voigt[1,2]

[1]~~G~~Deutsches Zentrum für Luft- und Raumfahrt (DLR), Institute of Atmospheric Physics, 82234 Oberpfaffenhofen, Germany~~erman Aerospace Center, 82234 Weßling, Germany~~
[2]Johannes Gutenberg University Mainz, 55099 Mainz, Germany
[3]Max Planck Institute for Chemistry, 55128 Mainz, Germany
[4]Karlsruhe Institute for Technology (KIT), 76021 Karlsruhe, Germany
[5]Faculty of Aerospace Engineering, Delft University of Technology, 2629 Delft, Netherlands
[6]Deutsches Zentrum für Luft- und Raumfahrt (DLR), Flight Experiments, 82234 Oberpfaffenhofen, Germany

Correspondence to: Laura Tomsche (ltomsche@uni-mainz.de)

Abstract. Sulfur compounds in the upper troposphere and lower stratosphere (UTLS) impact the atmosphere radiation budget, either directly as particles or indirectly as precursor gas for new particle formation. In situ measurements in the UTLS are rare, but are important to better understand the impact of the sulfur budget on climate. The BLUESKY mission in May/June 2020 explored an unprecedented situation. 1) The UTLS experienced extraordinary dry conditions in spring 2020 over Europe, in comparison to previous years and 2) the first lockdown of the COVID-19 pandemic caused major emission reductions from industry, ground, and airborne transportation. With the two research aircraft HALO and Falcon, 20 flights were conducted over Central Europe and the North Atlantic to investigate the atmospheric composition with respect to trace gases, aerosol, and clouds. Here, we focus on measurements of sulfur dioxide (SO_2) and particulate sulfate (SO_4^{2-}) in the altitude range of 8 to 14.5 km which show unexpectedly enhanced mixing ratios of SO_2 in the upper troposphere and of SO_4^{2-} in the lowermost stratosphere. In the UT, we find SO_2 mixing ratios of (0.07±0.01) ppb, caused by the remaining air traffic, reduced SO_2 sinks due to low OH and low cloud fractions, and to a minor extend by uplift from boundary layer sources. Particulate sulfate showed elevated mixing ratios of up to 0.33 ppb in the LS. We suggest that the eruption of the volcano Raikoke in June 2019, which emitted about 1 Tg SO_2 into the stratosphere in northern midlatitudes caused these enhancements, in addition to Siberian and Canadian wildfires and other minor volcanic eruptions. Our measurements can help to test models and lead to new insights in the distribution of sulfur compounds in the UTLS, their sources and sinks. Moreover, these results can contribute to improve simulations of the radiation budget in the UTLS with respect to sulfur effects.

Formatiert: Deutsch (Deutschland)
Formatiert: Deutsch (Deutschland)
Formatiert: Deutsch (Deutschland)

1 Introduction

The stratospheric aerosol layer changes in time, especially after volcanic eruptions with plume injection heights into the stratosphere, the layer gets more pronounced (Kremser et al., 2016). It plays a role in the radiative balance and thus impacts the climate (Solomon et al., 2011). An enhanced aerosol concentration leads to a larger albedo. The geo-engineering community investigates the enhancement of the aerosol layer with injections of sulfur compounds into the stratosphere to partly counteract greenhouse gases related global warming (Crutzen, 2006; Schäfer et al., 2015). The stratospheric aerosol layer is often referred to as "Junge layer" and can extend from the tropopause up to 25 km (Junge et al., 1961). The chemical composition of the stratospheric aerosol layer is dominated by sulfate (SO_4^{2-}) particles, which consist mainly of pure sulfuric acid droplets, sulfuric acid with material from ablated meteoroids or mixed organic-sulfate particles (Murphy et al., 2014; Cziczo et al., 2001; Schneider et al., 2021). During volcanic quiescent periods, precursor gases, like carbonyl sulfide (OCS), and non-volcanic sulfur dioxide (SO_2), as well as tropospheric SO_4^{2-} particles preserve the stratospheric layer (Brock et al., 1995). Due to its long lifetime, OCS is vertically uplifted from the tropics into the stratosphere and there it converts mostly through photodissociation to SO_2 (Sheng et al., 2015). The SO_2 chemistry and transport depends strongly on the ambient conditions. In the free troposphere and lower stratosphere, SO_2 reacts predominantly with hydroxyl (OH) to sulfuric acid (H_2SO_4) (English et al., 2011; Stockwell and Calvert, 1983), thus the lifetime correlates with the OH concentration. At cold temperatures and in the presence of water vapour, the gaseous H_2SO_4 condenses quickly to particles (Almeida et al., 2013; Kirkby et al., 2011), thereby forming sulfate aerosol. In the boundary layer, pollution could significantly reduce the lifetime to hours (Lee et al., 2011) and consequently, also the transport of SO_2 to higher altitudes. Clouds could also limit the SO_2 lifetime to hours or days (Lelieveld et al., 1993), as the conversion of SO_2 to H_2SO_4 is faster in cloud droplets than in the gas phase (Seinfeld and Pandis, 2006). Nevertheless, SO_2 can be transported from the planetary boundary layer (PBL) into the UTLS region via different pathways. Similar to OCS, SO_2 can be vertically transported across the tropical tropopause layer (TTL) or by overshooting convection in the tropics (Fueglistaler et al., 2009) or by the transport of SO_2 in a warm conveyor belt (WCB) in the midlatitudes (Arnold et al., 1997; Clarisse et al., 2011; Fiedler et al., 2009) or by transport processes connected with the Asian monsoon (Gottschaldt et al., 2017, 2018; Ploeger et al., 2017; Tomsche et al., 2019; Vogel et al., 2019; von Hobe et al., 2021). An explosive volcanic eruption can inject huge amounts of ash, SO_2, and other volcanic gases into the stratosphere and thus enhance the stratospheric aerosol layer (Kremser et al., 2016). In 1991, the volcano Mount Pinatubo (15°N) emitted approximately 20 Tg of SO_2 and 30 Tg of aerosol (McCormick et al., 1995), which impacted the stratosphere globally. Volcanic eruptions in midlatitudes can also impact the stratosphere, e.g. Mount St Helens (46°N, SO_2=0.8 Tg) in 1980, but its impact vanished in about a year (Deshler et al., 2006). One recent midlatitude eruption of similar strength was the volcano Raikoke in June 2019 (48.28°N, Kloss et al., 2021, de Leeuw et al., 2021) which emitted approx. 1.4-1.6 Tg SO_2. A further important source of stratospheric aerosol are intense wildfires, which can potentially develop pyrocumulonimbus (pyroCb) and thus transport biomass burning emissions into the UTLS (Fromm et al., 2005; Peterson et al., 2018). Moreover, air traffic is another source of particles and precursor gases in the UTLS (Lee et al., 2010; Voigt et al., 2010; Jurkat et al., 2011).

Feldfunktion geändert

Feldfunktion geändert

Feldfunktion geändert

In late spring 2020, the UTLS region was probed over Europe during the BLUESKY mission, the period covered the first weeks of the COVID19 lockdown in Europe, which caused reductions in emissions from industry, ground, and especially airborne transportation (Voigt et al., 2022). Under these conditions, we found enhanced values of SO_2 in the upper troposphere (UT) and of particulate SO_4^{2-} in the lowermost stratosphere (LS), which motivated us to investigate these sulfur compounds with respect to their sources and sinks.

In the following, we first present the BLUESKY mission in section 2. In section 3.1, we introduce the airborne measurements and in section 3.2 the trace gas and particulate profiles obtained during BLUESKY and also show tropospheric and stratospheric influenced compounds in tracer-tracer correlations (section 3.3). Afterwards, we focus on the SO_2 profile in the UT (section 4) and continue in section 5 with the stratospheric sulfate aerosol. Finally, we summarize our results and give an outlook in section 6.

2 Methods

2.1 BLUESKY mission

The BLUESKY mission was led by the German Aerospace Center (DLR) and the Max-Planck-Institute for Chemistry, Mainz. Coordinated flights were performed from Oberpfaffenhofen with the High-Altitude and Long-Range Research Aircraft HALO and the DLR Falcon over Europe and the North Atlantic between 16 May and 09 June 2020. In total 20 flights were performed (Fig. 1). The period covered the first weeks of the COVID-19 lockdown in Europe and thus offered a unique opportunity to investigate an unprecedented situation of reduced anthropogenic emissions from industry, ground, and airborne transportation. The goal of BLUESKY was to explore the changes in the atmospheric composition and gain new insights on how anthropogenic emissions perturb chemical and physical processes in the atmosphere. Both aircraft were equipped with in situ instruments to investigate trace gases, aerosols, and cloud properties. The payload of both aircraft was complementary to obtain a comprehensive dataset. Especially, during five days with coordinated flights over Germany (23 May, 26 May, and 28 May) and over the North Atlantic (30 May, 02 June), the payload offered the opportunity to probe the air masses in more detail. An overview of the BLUESKY mission is given in Voigt et al. (2022) and further detailed studies are published by Schumann et al. (2021a, 2021b), Reifenberg et al. (2021), Nussbaumer et al. (2021), Hamryszczak et al. (2022) and Krüger et al. (2022). In the present study we will focus on the sulfur compounds in the upper troposphere and lower stratosphere.

Formatiert: Englisch (Vereinigte Staaten)
Feldfunktion geändert
Formatiert: Englisch (Vereinigte Staaten)
Feldfunktion geändert
Formatiert: Englisch (Vereinigte Staaten)
Feldfunktion geändert
Formatiert: Englisch (Vereinigte Staaten)
Feldfunktion geändert
Formatiert: Englisch (Vereinigte Staaten)
Formatiert: Englisch (Vereinigte Staaten)
Formatiert: Englisch (Vereinigte Staaten)
Formatiert: Englisch (Vereinigte Staaten)

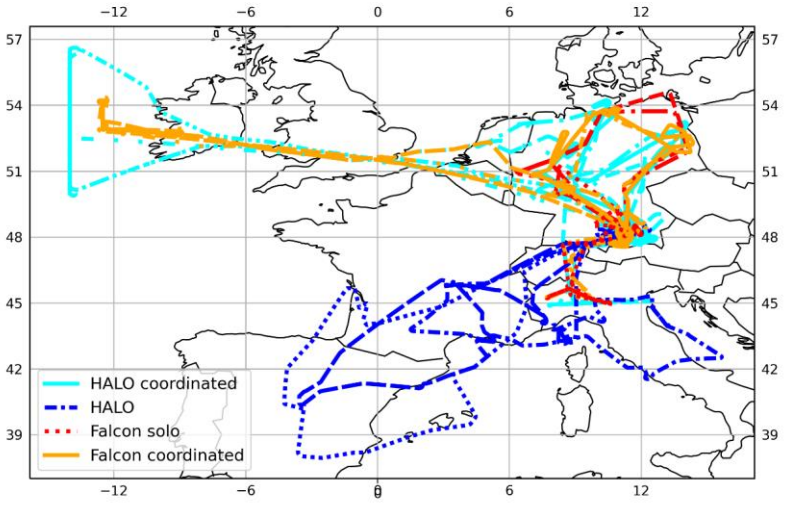

Figure 1: Overview of all flight tracks performed by Falcon (red) and HALO (blue) during the BLUESKY mission in May/June 2020 during the COVID19 lockdown. Coordinated flights (Falcon: orange; HALO: cyan) were performed over Germany on 23 May, 26 May, and 28 May and twice (30 May and 02~~nd~~ June) as both aircraft headed towards the North Atlantic, west of Ireland.

2.2 Instrumentation

In the present study several trace gas measurements onboard Falcon and also trace gas and particle measurements onboard HALO are used. Onboard Falcon, the atmospheric chemical ionization mass spectrometer AIMS measures gaseous SO_2 and nitric acid (HNO_3) among other compounds at mixing ratios relevant for the UTLS region by using SF_5^- as reagent ion. A more detailed description of the instrument can be found elsewhere (Voigt et al., 2014; Jurkat et al., 2016; Marsing et al., 2019). SO_2 is calibrated in–flight using an isotopically labelled calibration gas mixture of the isotope $^{34}SO_2$, which is heavier than the naturally dominant isotope $^{32}SO_2$, but has the same chemical behaviour (Jurkat et al., 2016). The natural isotopic ratio is $^{34}S/^{32}S$ =0.0454 and the mass spectrometer can detect both isotopes separately as they differ in mass by 2 amu (atomic mass units). This has the advantage that the calibration gas can be continuously added to the sampling flow and the

system is well conditioned for SO_2. A drawback is that the background of the instrument is increased by 5%, due to impurities of $^{32}SO_2$ in the calibration gas. The SO_2 data are instrument background corrected, which includes a moisture correction, as higher water vapour concentrations lead to cross sensitivities on *m/z* =83 amu (FSO_2^-; Jurkat et al., 2016). With increasing moisture in lower altitudes, a correction is more difficult and reduces the data quality. As the focus of the present study is the UTLS region, we limited our analysis ~~, thus we focus~~ on altitudes above 8 km and thus ensure the data quality. The other trace gas measured by AIMS is HNO_3, which is in-flight calibrated using a permeation oven with a solution of HNO_3 in water (Jurkat et al., 2014). The data are background corrected including a moisture correction, which is necessary to account for cross sensitivities caused by water vapour (Jurkat et al., 2016). The AIMS measurements were performed with a 1.6 sec time resolution and smoothed with a running mean of 20 seconds. The 1 σ detection limit of SO_2 varied between 0.006-0.017 ppb. The total uncertainty is on average 22.7% for SO_2 and included the uncertainty of the moisture correction. The 1-σ detection limit for HNO_3 is in the range of 0.005-0.009 ppb. The HNO_3 total uncertainty is on average 16% (Marsing, 2021). Further measurements onboard Falcon included CO and O_3. O_3 was measured using a UV photometer (Schulte and Schlager, 1996; Ziereis et al., 2000), CO was measured by cavity ring down spectroscopy (Klausner et al., 2020). The accuracies for CO and O_3 are 15% and 5%, respectively. Additionally, water vapor (H_2O) was measured with the lyman-alpha absorption instrument integrated in the meteorological sensor system.

Onboard HALO, the compact time-of-flight aerosol mass spectrometer (C-ToF-AMS) measured the aerosol composition (Drewnick et al., 2005; Schmale et al., 2010; Schulz et al., 2018). Aerosol particles of approximately 50 to 800 nm are analysed, which then provides quantitative mass concentrations of organic matter, sulfate, nitrate and ammonium. The instrument is equipped with a constant pressure inlet that ensures a steady mass flow and an operation pressure of the aerodynamic lens for stable inflight operation (Molleker et al., 2020). Here, we focus on sulfate. For a better comparability of SO_4^{2-} with SO_2, we calculate mixing ratios (ppb) instead of using concentrations (µg m^{-3}). Additionally, mixing ratios have the advantage of being pressure independent. We assumed that all SO_4^{2-} would be evaporated and calculated the volumetric mixing ratio for SO_4^{2-}. Above 8 km, the 1 σ detection limit is (0.006 ± 0.001) ppb for SO_4^{2-}, the accuracy is 30% and the precision on average (0.002±0.001) ppb (Schulz et al., 2018). Additionally, the trace gases CO and O_3 onboard HALO are considered in the present study for altitudes above 8 km. CO was measured by the TRacer In-Situ Tdlas for Atmospheric Research (TRISTAR; Schiller et al., 2008) with a total uncertainty of 3 % for tropospheric measurements (Nussbaumer et al., 2021). Note that due to a small Nitrous oxide (N_2O) interference the uncertainty in the lower stratosphere is higher (8.5 ± 3.9 ppbv). O_3 was measured by the Fast Airborne Ozone instrument FAIRO, which combines the technique of a UV photometer and a chemiluminescence detector (Zahn et al., 2012). The O_3 total uncertainty was 2-2.5%. Water vapor was measured with the tunable diode laser (TDL) hygrometer SHARC (Sophisticated Hygrometer for Atmospheric ResearCh).

SO_2 was sampled onboard Falcon and SO_4^{2-} was probed onboard HALO. Nevertheless, campaign averaged CO and O_3 profiles from both aircraft agree and motivate the combined interpretation of the SO_2 and SO_4^{2-} distributions during spring 2020 (see Sec. 3.2).

Formatiert: Schriftart: (Standard) +Überschriften (Times New Roman), 10 Pt.

Formatiert: Tiefgestellt

2.3 Trajectory calculations

Back trajectory calculations were performed using the HYSPLIT atmospheric transport and dispersion model (Stein et al., 2015; Rolph et al., 2017) with the GDAS (Global Data Assimilation System) meteorological dataset. For selected cases with either elevated SO_2 or SO_4^{2-} mixing ratios, 360 h back trajectoryies ensembles were calculated for nine starting points. We used three locations (longitude/latitude) along the flight track, which reflect before, at, and after the event, and for each location, we varied the altitude to 8000, 10000, and 12000 m.One ensemble consists of 27 single trajectories, which are offset by one meteorological grid point in the horizontal and 0.01 sigma in the vertical coordinate. With the help of the back trajectories, air mass origins and transport pathways in the atmosphere could be identified.

3 Results

3.1 Trace gases along flight track

On 02 June 2020, HALO and Falcon took off in Oberpfaffenhofen and headed towards the North Atlantic, west of Ireland, with similar flight tracks, altitude and similar take-off time. With a shorter flight range, Falcon landed in Shannon/ Ireland to refuel, while HALO continued its flight. In Figure 2, flight altitude and in situ measurements are plotted against longitude for comparability from both aircraft for the time between 7:00 and 10:00 UTC. O_3 and CO were measured aboard both aircraft. Both trace gases show similar patterns independent of the aircraft. The highest O_3 mixing ratios with maxima of 475 ppb (Falcon) and 423 ppb (HALO) were approximately between 6°W and 3°E, while CO had the lowest mixing ratios of 18 ppb (Falcon) and 28 ppb (HALO) and vice versa along the same longitudes outside this rangeand vice versa, when CO mixing ratios were enhanced with maxima of 110 ppb (Falcon) and 109 ppb (HALO), O_3 mixing ratios were low (Falcon: 74 ppb, HALO: 62 ppb). Because CO and O_3 from both platforms agree within their uncertainties and reflect the same trends, we assume that both aircraft probed the same air mass. Between 6°W and 3°E, O_3 and HNO_3 are positively correlated, as expected, reflects the O_3 behaviour quite well, and with enhanced HNO_3 mixing ratios increase up to 1.6 ppb in the mentioned longitude range. A similar trend can be observed in the particulate compound SO_4^{2-}, which also is enhanced when O_3, as a stratospheric tracer, is enhanced. SO_4^{2-} ranges from the detection limit to 0.21 ppb. SO_2 mixing ratios show a larger variability, but in general, they follow the CO mixing ratios, which is a tropospheric tracer (Fischer et al., 2000; Hoor et al., 2002). SO_2 ranges from the detection limit to 0.15 ppb and experiences one short peak with 0.15 ppb around 6.5°W at an altitude of 11.9 km. Other trace gases onboard Falcon measured to 266 ppb O_3, 70 ppb CO, and 0.8 ppb HNO_3 during this event, but beside HNO_3, which increased slightly, CO and O_3 showed no perturbations around this location. An in-depth analysis and discussion on potential explanations for this or similar features will follow in sections 4.Back trajectory analysis (Fig. 5i) indicate mostly long-range transport at high altitudes.

Formatiert: Tiefgestellt

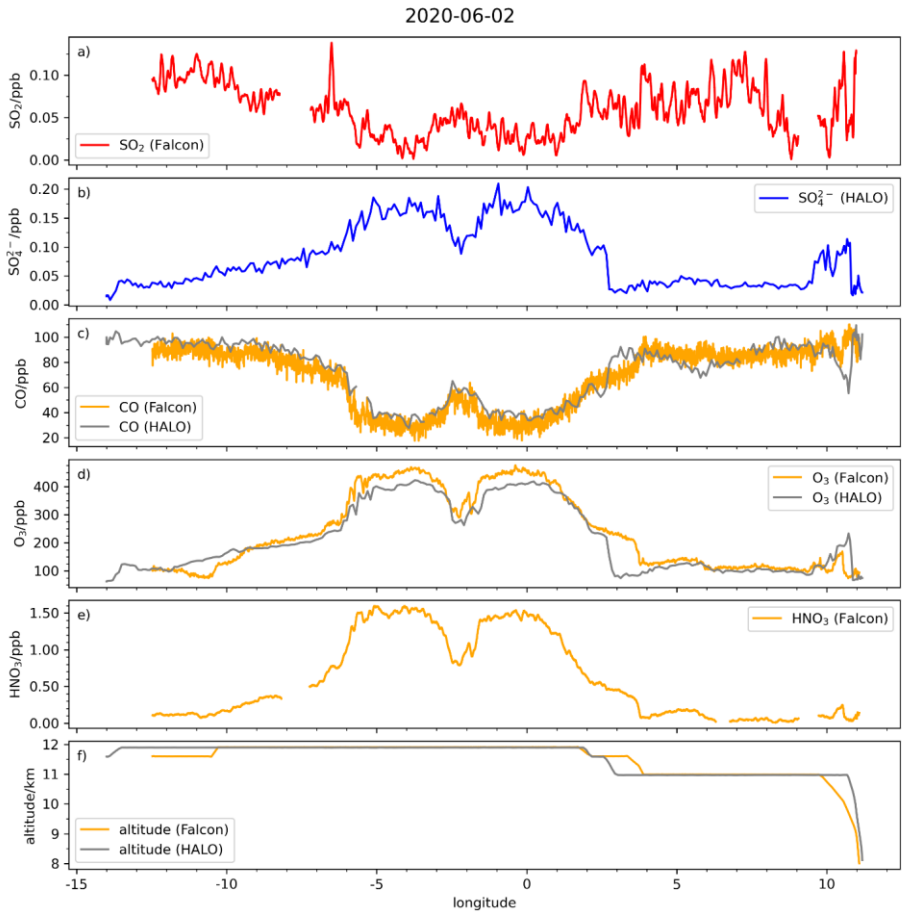

Figure 2: On 02 June 2020, HALO and Falcon had similar flight tracks from Oberpfaffenhofen towards the North Atlantic, west of Ireland. The sampling was roughly between 7-10 UTC. Plotted are in a) SO_2, b) SO_4^{2-} c) CO, d) O_3, e) HNO_3 and f) altitude.

170

3.2 SO_2 and SO_4^{2-} median profiles

Following the case mentioned above, we broaden our analysis to all flights of the whole campaign. In Figure 3, median, 25th and 75th percentile profiles of the trace gases and the particulate compounds are displayed with the potential temperature as a vertical axis. The medians, 25th and 75th percentiles are calculated for 5 K potential temperature bins from 310 K to 355 K for Falcon flights and up to 385 K for HALO flights. The Falcon profile is limited in height due to the maximum flight altitude of approx. 12.5 km in comparison to HALO with a ceiling altitude of 14.5 km. First, we compare the trace gases measured on both aircraft, Falcon and HALO. The stratospheric tracer O_3 behaves similar for both aircraft within the 25th and 75th percentiles with a step around 340 K, while the spread between the percentiles starts to increase already around 330 K. Below this altitude, median O_3 mixing ratios reach minima of 41 ppb (Falcon) and 62 ppb (HALO) and above they rise up to 420 ppb (Falcon) and 642 ppb (HALO). The chemical tropopause is marked by strong gradients in several tracers. O_3 as a common indicator shows a kink in its median profile at around 140 ppb and 340 K potential temperature, which is within the limits given by Thouret et al. (2006)~~According to Thouret et al. (2006), we use a O_3 threshold of 120 ppb as the chemical tropopause, which corresponds here to a potential temperature of 330 K, even though most tracers experience a stepwise increase around 340 K~~. The dynamical tropopause, displayed as the 2 PVU based on ECMWF/ERA5 data along the Falcon flight tracks (Fig. 3), is around 335 K and thus has a similar height as the chemical tropopause. The tropospheric tracer CO from both platforms has similar profiles with median mixing ratios of 37-112 ppb (Falcon) and 12-96 ppb (HALO). Both CO profiles show a decrease with height, thus anticorrelated to O_3, but they reflect a significant change in the mixing ratios at 340 K, similar to O_3. The profiles of the tropospheric tracer H_2O also decrease with height, following the CO profile, but with a less pronounced step around the chemical tropopause. The H_2O mixing ratios are 26-268 ppb (Falcon) and 3-153 ppb (HALO). Additionally, the median HNO_3 profile follows the trend of O_3 with low mixing ratios down to 0.3 ppb followed by a steep increase around 340K and reaches a maximum of 1.4 ppb. Between 330 K and 350 K, the stratospheric tracers O_3 and HNO_3, as well as the tropospheric tracer CO show larger variations between the percentiles, which indicates the mixing layer described by Hoor et al. (2002) over the course of the mission. As shown, the profiles for O_3 and CO for HALO and Falcon flight tracks agree well within their 25th and 75th percentiles. Both aircraft probed the atmosphere above Europe and the North Atlantic within the mission period and thus during similar meteorological conditions, even though the days and routes partly differ. This gives us confidence to further investigate and compare measurements of sulfur compounds sampled on both aircraft: SO_2 was sampled on Falcon, while SO_4^{2-} was probed on HALO. Profiles of SO_2 and SO_4^{2-} are shown in Fig. 3a and 3b, respectively. The median SO_2 profile decreases with height and median values range from 0.05 ppb to 0.08 ppb with the lowest mixing ratios above 330 K. The opposite behaviour can be observed in the median SO_4^{2-} profile, which increases with height. The mixing ratios are lowest at 0.02 ppb and raise up to 0.33 ppb. The profile shows a similar

Formatiert: Tiefgestellt

Formatiert: Tiefgestellt

trend in comparison to O_3 with a stepwise increase around 340 K. The enhanced SO_4^{2-} mixing ratios above the chemical tropopause can be associated with ~~the~~ stratospheric sulfate aerosol.

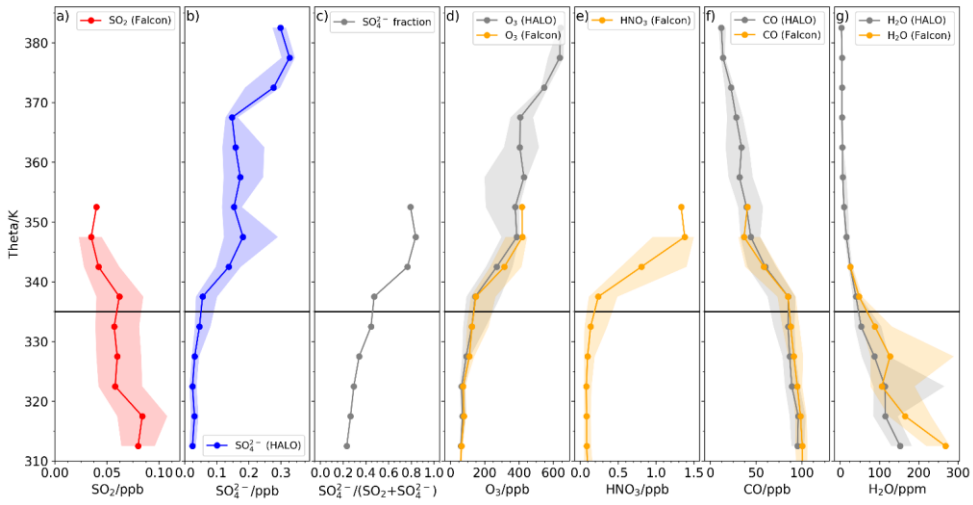

Figure 3: Median profiles with 25th and 75th percentiles as shaded areas are shown for trace gases with the potential temperature as vertical axes. The data are calculated for 5K potential temperature bins. In: a) SO_2, b) SO_4^{2-}, c) the SO_4^{2-} / ($SO2+ SO_4^{2-}$) ratio d) O_3, e) HNO_3, ~~and~~ f) CO, and g) H_2O for measurements performed on HALO and Falcon. Additionally, the black line at 335 K roughly indicates the dynamical tropopause (as 2PVU) based on ECMWF/ERA5 analysis along the Falcon flight tracks.

Formatiert: Tiefgestellt

In Figure 3c the profile of the ratio of SO_4^{2-}/(SO_2+ SO_4^{2-}) is plotted. The ratio is a measure of the relative contribution from the precursor SO_2 to the total sulfur budget. Below the chemical tropopause most of the SO_2 is still present as SO_2, while above the tropopause SO_4^{2-} dominates the ratio. The sum of SO_2 and SO_4^{2-} for the median profiles is rather stable around 0.10 ppb between 310 K and 340 K, above the sum increases up to on average 0.20 ppb and is dominated by the enhancement of SO_4^{2-} in the range 340-355 K. In the next section we will discuss potential sources explaining the distribution of sulfur compounds in the UTLS.

3.3 Stratospheric and tropospheric influenced air masses

In order to obtain an overview on the distribution of sulfur compounds with respect to the chemical tropopause, Fig. 4 shows tracer-tracer correlations of O_3, CO, and HNO_3, comparable to previous studies investigating the cross-tropopause exchange

and the chemical composition of the tropopause (Fischer et al., 2000; Hoor et al., 2002). In contrast to the median profiles in the previous section, here all available data are plotted, either for HALO (considering SO_4^{2-}) or for Falcon (considering SO_2). In the correlation plot between O_3 and CO color-coded with SO_4^{2-} (Fig. 4a) from HALO for the whole altitude range (0-14 km), the stratospheric branch is visible with low CO and high O_3 values, while the tropospheric branch is characterised by low O_3 and high CO values, similar to e.g. Fischer et al., (2000). The transition layer is clearly visible, the layer is a mixing layer, influenced by air masses with stratospheric and tropospheric origin (Hoor et al., 2002). Without the exchange processes across the tropopause, we would expect a L-shape profile (Fischer at al., 2000). The mixing layer almost extends over the whole O_3 range from 150 ppb to 400 ppb, similar to other mixing layers in the same latitude and season (Hoor et al., 2002; Pan et al., 2004) and thicker in comparison to a winter polar mixing layer (Fischer et al., 2000). The higher SO_4^{2-} mixing ratios are either in the (unmixed) stratospheric branch or partly mixed into in the upper part of the transition layer. With respect to the chemical tropopause, the elevated SO_4^{2-} mixing ratios appear only in the stratosphere ($O_3 \geq 120$ ppb; Thouret et al., 2006). In Figure 4b) the correlation between O_3 and CO with and without color-coded SO_2 onboard Falcon is displayed. A subset of the Falcon flights is missing there due to missing O_3 data in the beginning of the campaign. As the Falcon mainly operated up to 12 km, the pure stratospheric branch is hard to identify, while the tropospheric branch is clearly identifiable with the black dots (without SO_2). However, within the mixing layer, the stratospheric and tropospheric influences still differ, which is reflected in the SO_2 mixing ratios. In order to cover all Falcon flights, we use here HNO_3 as a stratospheric tracer. In Figure 4c, the HNO_3 to CO correlation for the measurements onboard Falcon are plotted with color-coded SO_2, the Figure includes all Falcon flights, Figure 4b and 4c show similar patterns for SO_2, with higher mixing ratios towards more tropospheric influence and lower mixing ratios when the stratospheric influence dominates. ~~Some~~ One SO_2 outlier~~s~~ with higher mixing ratios at enhanced HNO_3 und reduced CO can be identified (Fig. 4c; grey circle). A possible explanation could be (aged) aircraft plume encounters (as observed e.g. in Jurkat et al., 2011), as HYSPILT back trajectory calculations tend towards long range transport in the UTLS region for thi~~sese~~ case~~s~~ (Fig. 5a/b). ~~Furthermore~~Generally, the trajectories do not indicate transport from local PBL sources for cases with elevated SO_2. In Figure 5a-h, examples for cases with elevated SO_2 are shown, including the case on 02 June 2020 described in section 3.1 (Fig. 5g/h). Additionally, Hamryszczak et al. (2022) found that hydrogen peroxides were scavenged by clouds during BLUESKY in the lower and middle troposphere (0-7 km). As SO_2 can easily be scavenged by clouds (Seinfeld and Pandis, 2006), the potential for SO_2 being transported from the local PBL to the UT seems unlikely. The tracer-tracer-correlation and the relative distribution of SO_2 along the transition layer show no direct link to the SO_4^{2-} distribution, as they are in different regimes, thus we assume that they originate from different sources. The back trajectories of SO_2 and SO_4^{2-} cases support the assumption that the origins differ, especially concerning the different altitude ranges of the trajectories (Fig. 5).

Formatiert: Tiefgestellt

Formatiert: Tiefgestellt

Formatiert: Tiefgestellt

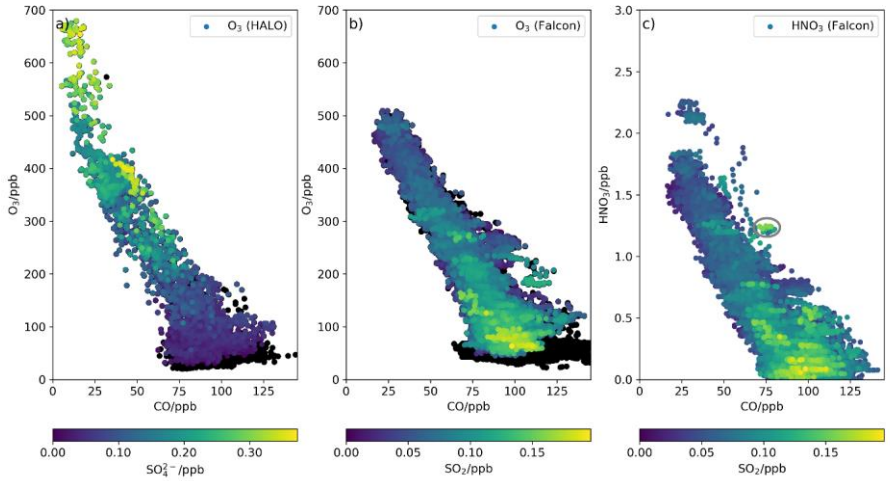

Figure 4: Tracer-tracer correlation for a) 30 sec data CO - O_3 in black for whole altitude range and for heights above 8 km SO_4^{2-} is~~with~~ color-coded ~~SO_4^{2-}~~ from HALO flights, b) CO - O_3 in black for whole altitude range, and with color-coded SO_2 (above 8 km) from Falcon flight, when O_3 was available, and c) 1 sec data CO - HNO_3 with color-coded SO_2 from Falcon flights. In c) a grey circle marke~~s~~ an outlier with high SO_2, CO and HNO_3.

Formatiert: Tiefgestellt

Formatiert: Tiefgestellt

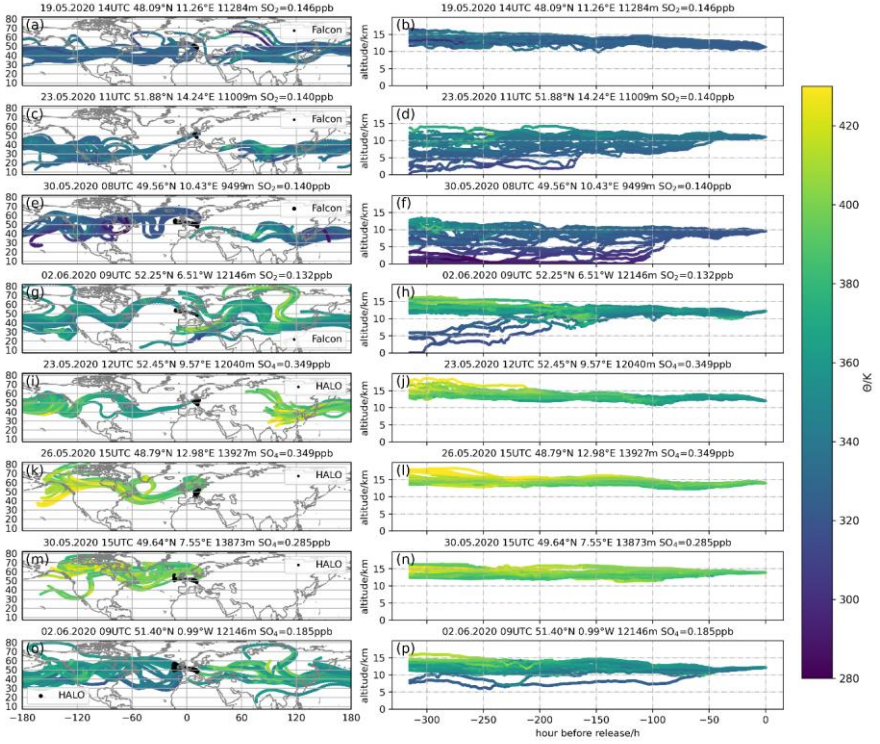

Figure 5: HYSPLIT 360 hours back trajectories calculated for cases with elevated SO_2 (a-h; Falcon) and SO_4^{2-} HNO_3 (i-p; HALO) mixing ratios, while CO was reduced. The release points started in the vicinity of these events. In the left column: In black are the flight tracks, color-coded is the potential temperature along the trajectories to indicate display the transport altitude. The right column represents the trajectories as hours before release vs. altitude, also with color-coded potential temperature Further, some events display transport of PBL air masses with origins in Asia, the east coast of the US, or the Caribbean, which is lifted to the UTLS region and then transported at high altitudes towards the measurement region. The cases of enhanced SO_2 were on 19 May 2020 (a, b), 23 May 2020 (c, d), 30 May 2020 (e,f), and 02 May June 2020 (eg, h). The cases of elevated SO_4^{2-} were on 23 May 2020 (i, jd), 26 May 2020 (ek, l), 30 May 2020 first flight (f) and second flight (gm, n), and 02 June 2020 (ho, p) and 02 June 2020 (i).

4 Enhanced SO_2 in the UT

In Figure 6a, the median SO_2 profile with shaded 25th and 75th percentile is plotted against the flight altitude, in order to compare the data with literature values. The SO_2 percentiles are calculated for 500 m bins. Similar to Fig. 3b, the median SO_2 decreases with height from around 0.08 ppb to 0.04 ppb. Previous in situ SO_2 measurements at similar flight altitudes are included in Fig. 6a. Overall, the BLUESKY SO_2 measurements are within the range of previous airborne studies, even though all studies are snapshots of the atmosphere of different locations on the Northern hemisphere, different seasons, and different meteorological situations. Keeping this in mind, we will have a closer look. Williamson et al. (2021) reported low mixing ratios for the remote Northern hemispheric background over the Pacific for the upper troposphere as well as for the lowermost stratosphere during the ATom mission (2016-2018). Speidel et al. (2007) reported higher SO_2 values for the upper tropospheric background over Europe and the eastern Atlantic in summer 2004. Jurkat et al. (2010) measured the stratospheric background over Europe in autumn 2008 in a similar range to Speidel et al. (2007). Above 12 km the BLUESKY SO_2 mixing ratios agree well with the stratospheric background from Jurkat et al. (2010) and the tropospheric background from Speidel et al. (2007). Surprisingly, the BLUESKY SO_2 profile slightly exceeds the previous measurements below these altitudes in the upper troposphere. The upper tropospheric SO_2 profile compares better to SO_2 mixing ratios, which were associated with the SO_2 background in the North Atlantic flight corridor in 1997 or 2010 (Arnold et al., 1997; Jurkat et al., 2010). Arnold et al. (1997) reported SO_2 mixing ratios in the range of 0.03-0.3 ppb in October 1993 during POLINAT and Jurkat et al. (2010) measured 0.09 ppb of SO_2 during CONCERT in autumn 2008. Due to implementation of SO_2 emission control policies, the global SO_2 emissions decreased since 1980 (Hoesly et al., 2018; Aas et al., 2019), nevertheless the sulfur content in kerosene remained unchanged (Lee et al., 2021; Miller et al., 2009), thus the aviation based SO_2 emissions depend on the air traffic.

In 2020, a 72% reduction of the air traffic above Europe has been reported due to the COVID19 lockdown in comparison to the same time period in 2019 (Schumann et al., 2021a, 2021b), hence providing a lower aviation SO_2 source with respect to 2019. Compared to 2010, the 3.5% increase in air traffic per year (Lee et al., 2011) promotes an increase by a factor of 1.5 of the 2010 air traffic for a scenario without COVID19 restrictions in 2020 and consequently a~~n~~ theoretical increase of 50 percent in aviation SO_2 emissions for 2020, given that the sulfur content of the kerosene is unchanged (Lee et al., 2021; Miller et al., 2009). In 2020, The ~~increase in air traffic~~ remaining air traffic of 28% (in comparison to 2019) corresponds to roughly 40% of the 2010 air traffic and might hence in part explain the SO_2 mixing rations detected in the upper troposphere, which are still higher than remote background measurements (Williamson et al., 2021).

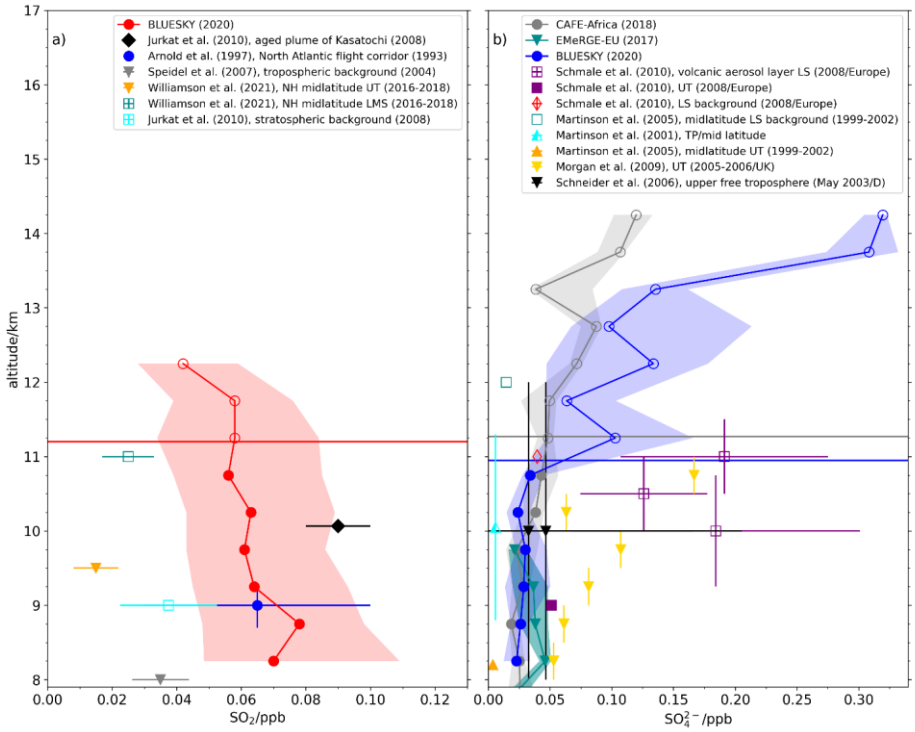

Figure 6: Profiles for a) SO_2 and b) SO_4^{2-} for 500m altitude bins. In a) additional literature SO_2 values are shown, while in b) literature values for SO_4^{2-} are added, including SO_4^{2-} profiles from previous HALO missions with the aerosol mass spectrometer C-ToF-AMS onboard: EMeRGe-EU in June/July 2017 (Andrés Hernández et al., 2022) and four flights over Europe of the CAFE-Africa mission in July-September 2018. Full markers are tropospheric origin and open markers are stratospheric origin. Additionally, the dynamical tropopause (~2PVU) along the Falcon tracks is marked as red horizontal line in a) and the thermal tropopause is marked as blue horizontal line for HALO tracks and in grey for CAFE-Africa in b).

In addition, further sources could have contributed to the SO_2 budget in the upper troposphere. To analyse the origin of air masses with elevated SO_2, HYSPLIT back trajectories are calculated and representative examples are plotted in Fig. 5a-h. SO_2 emissions from anthropogenic and natural sources in the PBL can be lifted to the UT via convection or via warm conveyor belts and transported to the measurement region. Arnold et al. (1997) reported an extended layer of enhanced SO_2

Formatiert: Tiefgestellt

with maxima of up to 3 ppb in the Northeast Atlantic, which was an air mass uplifted and transported from the polluted PBL from the eastern United States. A few cases show trajectories with similar pathways, like the example in Fig. 5e/f. Nevertheless, the PBL contacts are also over the Pacific and East Asia. The latter one suits better to the findings of Fiedler et al. (2009) who observed ~~Another possibility is~~ the uplift of polluted air masses from East Asia via warm conveyor belts and upper tropospheric long-range transport towards Europe ~~(Fiedler et al., 2009)~~. Further, the Asian monsoon also serves as a vertical transport pathway for emissions from the PBL up to high altitudes, where the air mass can enter the LS and horizontally be transported either eastwards (Vogel et al., 2014, 2016) or can be horizontally transported in the UT (Tomsche et al., 2019) and finally reach Europe. Similar ~~T~~trajectory pathways can be found for the cases in Fig. 5a/b and 5g/h. These trajectories indicate long range transport in the UT and could have been impacted by the Asian monsoon.~~analysis (Fig 5) for the BLUESKY period indicate some events of PBL air masses with origins in Asia, the east coast of the US, or the Caribbean lifted to the UTLS region and then being transported at high altitudes.~~ Generally, the trajectories with elevated SO_2 (Fig. 5a-h) show lower potential temperatures in comparison to the trajectories calculated for elevated SO_4^{2-} (Fig. 5i-p). Hence, long range transport of SO_2 enriched PBL air masses could have contributed to the observed BLUESKY SO_2 mixing ratios in the UT. Nevertheless, the decrease of SO_2 in the LS, as expected, does not support transport of SO_2 beyond the UT into the LS neither via convection nor warm conveyor belts. This can be confirmed by the trajectories for SO_4^{2-} as they indicate long range transport at high altitudes with negligible influence from lower altitudes. The trajectories helped identifying potential source regions of SO_2.

Beside the sources, also sinks of SO_2 can alter the SO_2 concentrations in the UTLS. Beside the conversion to H_2SO_4, leading to sulfate particles, SO_2 is removed from the atmosphere by wet and dry deposition. SO_2 can be scavenged by clouds, which lead to a significant reduction of the SO_2 lifetime (Lelieveld, 1993). Van Heerwaarden et al. (2021) investigated the meteorological situation in spring 2020 and found that a stable high pressure system over Europe lead to a lower cloud fraction in comparison to the mean 2010-2019 period over Europe. This would lead to less cloud processing and reduce SO_2 sinks. Furthermore, elevated humidity favours the faster conversion of SO_2 to SO_3 and sulfate, as water vapour enhances the potential for elevated OH concentrations (Pandis and Seinfeld, 2006). As reported by Schumann et al. (2021a, 2021b) the UTLS was drier in spring 2020 in Europe in comparison to previous years. The median H_2O profiles during BLUESKY reach only mixing ratios of up to 268 ppb in the upper troposphere (Fig. 3g), which is still within the range of typical springtime H_2O mixing ratios in the upper troposphere (e.g. Hegglin et al., 2009; Kaufmann et al., 2018). But van Heerwaarden et al. (2021) found with respect to humidity and cloud cover spring 2020 was amongst the springs with the lowest values. ~~Van Heerwaarden et al. (2021) describe the meteorology in spring 2020 as exceptionally dry and with a lower cloud fraction in comparison to the mean 2010-2019 period over Europe. Less cloud processing would reduce SO_2 sinks.~~ Thus~~Moreover~~, the lower available H_2O led to lower OH concentrations during BLUESKY period, which ~~would~~ impli~~es~~y less chemical processing and hence ~~would also~~a reduction of SO_2 sinks. Less SO_2 sinks could lead to an enhanced SO_2 lifetime in the UTLS and thus higher SO_2 mixing ratios.

Formatiert: Tiefgestellt

Formatiert: Tiefgestellt

Formatiert: Tiefgestellt

Formatiert: Deutsch (Deutschland)

Formatiert: Deutsch (Deutschland)

Formatiert: Tiefgestellt

Formatiert: Tiefgestellt

In sum, the enhanced SO_2 mixing ratios at cruise levels in Europe in spring 2020 can possibly be explained by a non-negligible aviation SO_2 contribution, WCB or convective transport from the boundary layer, followed by long range transport, and the prolonged SO_2 lifetime caused by the unusually dry UTLS conditions. Neither the sources nor the sinks could separately explain the SO_2 mixing ratios in the UTLS. Beyond that, we are not able to analyse in more detail the different amounts of the aforementioned factors and how they contribute to single flights.

Formatiert: Tiefgestellt

5 Stratospheric sulfate aerosol

As mentioned in section 3.2, SO_4^{2-} has a distinct profile with a steep increase at a potential temperature of 340 K, which refers here to around 11 km with respect to altitude (Fig. 6b). This altitude reflects also the thermal tropopause height during BLUESKY (Fig. 6b). Up to this altitude, the mixing ratio is rather constant, then it increases. Between 8-11 km O_3 mixing ratios are stable, and above O_3 increases. O_3 mixing ratio above 120 ppb indicates stratospheric air masses as mentioned above, thus the higher SO_4^{2-} mixing ratios above 11 km can be attributed to the stratosphere and hence associated with stratospheric aerosol. The layer between 11 and 13.5 km can be influenced from the stratosphere as well as the troposphere, as the data are averaged over a few weeks and varying meteorological conditions, which lead to a broadening of the 25th to 75th percentiles range. In Figure 4a, this layer represents the mixed layer. The SO_4^{2-} correlates well with O_3 for all flights, similar to the flight on 02 June 2020, presented in section 3.1 (Fig. 2).

Formatiert: Tiefgestellt

Previous studies investigated the sulfate aerosol in the UTLS region in northern hemispheric midlatitudes (Fig. 6b). The BLUESKY mixing ratios in the UT agree well with the observations by Schneider et al. (2006) during May 2003, which were partly influenced by aircraft exhaust plumes. The BLUESKY mixing ratios are lower than the UT background reported by Schmale et al. (2010). Martinson et al. (2001, 2005) observed significantly lower SO_4^{2-} mixing ratios in the European upper troposphere and tropopause region. The SO_4^{2-} profile (Morgan et al., 2009) obtained from April 2005 to September 2006 over the UK shows higher SO_4^{2-} concentrations compared to the BLUESKY measurements. Morgan et al. (2009) suggest that the elevated mixing ratios in the UT are the result of regional uplift of polluted air masses during stagnant meteorological conditions over the UK.

Sulfate was measured in two previous HALO missions with the aerosol mass spectrometer C-ToF-AMS in a similar altitude range and region. During EMeRGe-EU, seven research flights were conducted in June/July 2017 above Europe at altitudes up to 10 km (Andrés Hernández et al., 2022~~4~~). The SO_4^{2-} mixing ratio was on average (0.04 ±0.01) ppb and compares well to the BLUESKY SO_4^{2-} mean in the same altitude range below 10 km. The second HALO mission was CAFE-Africa in summer 2018 ~~and~~ which reached altitudes up to 14 km. Here, only data obtained over Europe (38° - 57°N and 14°W -16°E) are used for the comparison, which include two test flights and the ferry flights (27 July, 01 Aug, 07 Aug, and 07 Sept 2018; Voigt et al., 2022). For the CAFE~~É~~É-Africa subset the thermal tropopause was slightly higher than during BLUESKY (Fig. 6b). For the altitude range 8-11 km, the SO_4^{2-} mean was (0.03 ±0.01) ppb, similar to the BLUESKY value. Above 11 km in

the lower stratosphere, SO_4^{2-} raises to (0.09 ±0.03) ppb. Considering heights above the tropopause, i.e. with enhanced SO_4^{2-} mixing ratios, the stratospheric BLUESKY SO_4^{2-} concentrations are a factor of 2 to 3 higher than the observations in summer 2018.

In the following, we investigate the origin of the elevated stratospheric SO_4^{2-} mixing ratios during BLUESKY. As mentioned above, we calculated HYSPLIT back trajectories for cases of elevated SO_4^{2-}. In Figure 5i-p, representative examples of trajectories are displayed. The majority indicates long range transport at high altitudes with potential temperatures between 343 K and 465 K. While the lower range of the potential temperature is associated with midlatitude tropopause height, the upper values are clearly associated with the stratosphere. As only few trajectories indicate lower potential temperatures, we assume that the majority of elevated SO_4^{2-} is already in the stratosphere 360 h before sampling and hence influence from the troposphere is negligible. One major source of SO_4^{2-} in the stratosphere ~~are~~ is volcanic eruptions. One year before BLUESKY, the volcano Raikoke on the Kuril Islands (Russia, 48.29°N, 153.25°E) in the Western Pacific started to erupt on 21 June 2019 and continued for some days, it was categorised to volcanic explosivity index VEI≥4. Several explosive eruptions emitted a dense ash and SO_2 plume, which rose up to 19 km and 20 km on consecutive days (Hedelt et al., 2019), thus also injecting into the stratosphere. Based on TROPOMI analysis, de Leeuw et al. (2021) reported, that the eruption released 1.4-1.6 Tg SO_2 into the atmosphere and simulated also that approximately 0.9-1.1 Tg SO_2 thereof were injected into the stratosphere. Kloss et al. (2021) used satellite based OMPS (Ozone Mapping Profiler Suite Limb Profiler) stratospheric Aerosol Optical Depth (sAOD) to investigate the temporal evolution from before the Raikoke eruption until May 2020. Almost one year later, the sAOD was still higher than prior to the eruption. This suggests that elevated SO_4^{2-} measured in the stratosphere during BLUESKY was partly caused by the Raikoke eruption a year earlier. The eruption of Mount St Helens in 1980 was of comparable size, midlatitude location, and SO_2 emissions (Deshler et al., 2006) and its impact was also visible for almost a year. Still, other sources cannot be completely ruled out. For example, severe wildfires in Alberta/Canada developed pyro cumulus clouds in June 2019. The biomass burning emissions where uplifted into the lower stratosphere (Osborne et al., 2022). In July 2019, also severe fires in Siberia/Russia impacted the OPMS sAOD (Kloss et al., 2021). In comparison to the Raikoke eruption, these biomass burning contributions are of lower magnitude. Reifenberg et al. (2021) suggest that other small and medium sized volcanic eruptions from tropical latitudes, could have reached the stratosphere and thus impacted the stratospheric aerosol over Europe. One example is the volcano Taal on the Philippines (14.00°N, 120.99°E), which erupted on 12 January 2020, and its ash and gas plume rose up to around 10-15 km height (Global Volcanism Program, 2020. Report on Taal (Philippines)). The VEI was estimated to 3 and the SO_2 emissions estimated to 0.019 Tg (Liu et al., 2020). According to simulations of Reifenberg et al. (2021), the Taal eruption lead partly to an increase of SO_4^{2-} in the LS during BLUESKY.

The measured SO_4^{2-} mixing ratios in the LS agree with other volcano related in situ studies. The highest mixing ratios are reported by Schmale et al. (2010). They probed layers with enhanced SO_4^{2-} in October/November 2008 roughly 3 months after the eruption of Mount Kasatochi (erupted 08 August 2008, 52.18°N, 175.51°W, 1.5 Tg SO_2), with an injection height

Kommentiert [SJ1]: Schon akzeptiert und schon im proofreading, sollte also hoffentlich bald erscheinen

reaching into the stratosphere and additionally Mount Okmok (53.40°N, 168.17°W) erupted on 12 July 2008 (0.2 Tg SO_2, Carn et al., 2008). Jurkat et al. (2010) also measured enhanced SO_2 concentrations in the stratosphere in the 3 months-old Kasatochi plume during the CONCERT campaign (Voigt et al., 2010). Martinsson et al. (2009) reported particulate sulfur concentrations shortly after the Kasatochi eruption were 10 times higher than before the eruption and even 3-4 months after the eruption they were enhanced by a factor of 3. In contrast, during volcanic quiescent periods, like the period between 1997 and 2008 (Deshler, 2008) the SO_4^{2-} has reduced mixing ratios in the stratosphere, and Martinson et al. (2005) reported SO_4^{2-} mixing ratios of 0.01 ppb for the lower stratosphere for the years 1999-2002.

The enhanced SO_2 in the UT as described in section 4 and the longer SO_2 lifetime could possibly have a minor effect on the stratospheric sulfate aerosol. In these conditions, the SO_2 had more time to be transported into the LS and finally be transformed to SO_4^{2-}, adding to the SO_4^{2-} mixing ratios. But it seems unlikely, as the trajectories for elevated SO_4^{2-} (Fig. 5i-p) stay at high altitudes (and high potential temperatures) and thus mixing from the troposphere into the stratosphere is negligible. A few trajectories indicate a downward transport from higher altitudes, thus an origin deeper in the stratosphere (Fig. 5k/l), which could be a hint for OCS as SO_4^{2-} precursor. ~~Moreover,~~ OCS is transported within the Brewer Dobson Circulation from the upper stratosphere to the lower stratosphere and being transformed via SO_2 to H_2SO_4. According to Brühl et al. (2012), it is the most important source for maintaining the stratospheric aerosol layer in volcanic quiescent periods and also for BLUESKY, OCS oxidation adds to the stratospheric SO_4^{2-} background to some extent. Further, the Junge layer might also influence the SO_4^{2-} mixing ratios in the LS. Even though the Junge layer is most pronounced at higher altitudes (Junge et al., 1961), it could extend further down or due to the downward transport mentioned above (Fig. 5k/l) SO_4^{2-} could be transported downward from the Junge layer into our measurement altitudes and thus contribute to the elevated SO_4^{2-}.

6 Conclusion and outlook

We find elevated SO_4^{2-} mixing ratios in stratospheric air masses, and enhanced SO_2 mixing ratios in tropospheric air masses over Central Europe and the North Atlantic in spring 2020. The elevated SO_2 of 0.06 ppb in the UT agrees with SO_2 mixing ratios performed in the background of the North Atlantic flight corridor in 2008 (Jurkat et al., 2010) despite lower air traffic due to COVID-19 restrictions in 2020. ~~-~~The 3.5% increase in air traffic since 2010 in part compensates the air traffic reduction in 2020. ~~-~~In addition, exceptional dry weather conditions leading to a low cloud fraction and low OH concentrations in the UTLS in May 2020 (Schumann et al., 2021a, 2021b, Van Heerwaarden et al., 2021) reduced SO_2 sinks and increased SO_2 lifetime. Back trajectories provided indications of ~~O~~other boundary layer SO_2 sources from convective or WCB transport and further long-range transport in the UT, which could have contributed to a small extend.

In the LS, enhanced SO_4^{2-} mixing ratios were observed. In comparison to previous studies the SO_4^{2-} mixing ratios were clearly above SO_4^{2-} mixing ratios reported during volcanic quiescent periods (e.g. Martinson et al., 2001, 2005) and agreed with SO_4^{2-}

mixing ratios in volcanic impacted air masses (e.g. Schmale et al., 2010) measured at altitudes below 12 km. Compared to 2018, stratospheric SO_4^{2-} was significantly enhanced in 2020. The eruption of the volcano Raikoke injected 0.9-1.1 Tg of SO_2 into the stratosphere (de Leeuw et al., 2021) in June 2019. In May 2020, an enhanced sAOD still was observed by Kloss et al. (2021) in the northern hemisphere caused by the Raikoke eruption and to a smaller extend by severe biomass burning events from June/July 2019 in Siberia and Canada. Further, Reifenberg et al. (2021) found that the eruption of the tropical volcano Taal in January 2020 contributed to the enhanced SO_4^{2-} in the LS. We suggest these to be the primary sources of the enhanced stratospheric SO_4^{2-} concentrations measured during BLUESKY, because back trajectories mainly showed long range transport in the lower stratosphere.

Overall, the unprecedented BLUESKY mission was conducted during exceptional meteorological conditions and also reduced air traffic, both impacted the SO_2 mixing ratios in the UT due to changes in the emissions and also sinks. The enhanced stratospheric sulfate aerosol, which was observed, was likely impacted by the volcano Raikoke, and smaller sources.

Together with the observations of other sulfur compounds such as gaseous H_2SO_4 on HALO, which are still under evaluation, the unique and comprehensive data set of sulfur compounds allows to test our understanding of the sulfur chemistry in global models (Reifenberg et al., 2021).

In a broader context, the present results give new insights in the sulfur chemistry in the UTLS region with respect to limited sources and sinks. They help to better understand a) the sensitivity of SO_2 to missing sinks and b) the stratospheric aerosol and its dependence on perturbances and their lasting impacts. Both aspects are important to improve models, especially with respect to simulations of the Earth's radiation budget, because changes in the radiation balance in the UTLS impact feedback processes in the global climate.

Data availability

Data are available on request at the HALO data base at https://halo-db.pa.op.dlr.de/mission/119.

Author contribution

CV, TJW, HS, JL planned the flight experiment. AM, JL, KK, JS, MS, LR performed the in-flight measurements. KK and JS provided evaluated particulate data and previous campaign data and supported the analysis. AM provided supporting evaluation and assisted the analysis. FO, AZ, HF, LR provided supporting evaluation. SK supported the analysis. LT evaluated and analysed the data and prepared the manuscript with contributions from CV, AM, TJW, JS, KK, HF and SK. All co-authors commented on the manuscript.

Competing interests

The authors declare that they have no conflict of interest.

Acknowledgements

Laura Tomsche is funded by the Deutsche Forschungsgemeinschaft (DFG, German Research Foundation) – TRR 301 – Project-ID 428312742. The HALO flights during the BLUESKY mission were funded by the Max Planck Society. The authors gratefully acknowledge the NOAA Air Resources Laboratory (ARL) for the provision of the HYSPLIT transport and dispersion model and/or READY website (https://www.ready.noaa.gov) used in this publication. The authors thank Andreas Giez, Christian Mallaun, and Vladyslav Nenakhov for providing the water vapor measurement onboard HALO and Falcon, as well as Benedikt Steil for providing the ECMWF/ERA5 reanalysis data.

Kommentiert [SJ2]: Wenn du die Tropopausenhöhen daraus genommen hattest.

References

Aas, W., Mortier, A., Bowersox, V., Cherian, R., Faluvegi, G., Fagerli, H., Hand, J., Klimont, Z., Galy-Lacaux, C., Lehmann, C. M. B., Myhre, C. L., Myhre, G., Olivié, D., Sato, K., Quaas, J., Rao, P. S. P., Schulz, M., Shindell, D., Skeie, R. B., Stein, A., Takemura, T., Tsyro, S., Vet, R., Xu, X. (2019). Global and regional trends of atmospheric sulfur. *Scientific Reports*, *9*(1), 953. doi:10.1038/s41598-018-37304-0

Almeida, J., Schobesberger, S., Kürten, A., Ortega, I. K., Kupiainen-Määttä, O., Praplan, A. P., Adamov, A., Amorim, A., Bianchi, F., Breitenlechner, M., David, A., Dommen, J., Donahue, N. M., Downard, A., Dunne, E., Duplissy, J., Ehrhart, S., Flagan, R. C., Franchin, A., Guida, R., Hakala, J., Hansel, A., Heinritzi, M., Henschel, H., Jokinen, T., Junninen, H., Kajos, M., Kangasluoma, J., Keskinen, H., Kupc, A., Kurtén, T., Kvashin, A. N., Laaksonen, A., Lehtipalo, K., Leiminger, M., Leppä, J., Loukonen, V., Makhmutov, V., Mathot, S., McGrath, M. J., Nieminen, T., Olenius, T., Onnela, A., Petäjä, T., Riccobono, F., Riipinen, I., Rissanen, M., Rondo, L., Ruuskanen, T., Santos, F. D., Sarnela, N., Schallhart, S., Schnitzhofer, R., Seinfeld, J. H., Simon, M., Sipilä, M., Stozhkov, Y., Stratmann, F., Tomé, A., Tröstl, J., Tsagkogeorgas, G., Vaattovaara, P., Viisanen, Y., Virtanen, A., Vrtala, A., Wagner, P. E., Weingartner, E., Wex, H., Williamson, C., Wimmer, D., Ye, P., Yli-Juuti, T., Carslaw, K. S., Kulmala, M., Curtius, J., Baltensperger, U., Worsnop, D. R., Vehkamäki, H., Kirkby, J. (2013). Molecular understanding of sulphuric acid–amine particle nucleation in the atmosphere. *Nature*, *502*(7471), 359-363. doi:10.1038/nature12663

Andrés Hernández, M. D., Hilboll, A., Ziereis, H., Förster, E., Krüger, O. O., Kaiser, K., Schneider, J., Barnaba, F., Vrekoussis, M., Schmidt, J., Huntrieser, H., Blechschmidt, A. M., George, M., Nenakhov, V., Harlass, T., Holanda, B. A., Wolf, J., Eirenschmalz, L., Krebsbach, M., Pöhlker, M. L., Kalisz Hedegaard, A. B., Mei, L., Pfeilsticker, K., Liu, Y., Koppmann, R., Schlager, H., Bohn, B., Schumann, U., Richter, A., Schreiner, B., Sauer, D., Baumann, R., Mertens, M., Jöckel, P., Kilian, M., Stratmann, G., Pöhlker, C., Campanelli, M., Pandolfi, M., Sicard, M., Gómez-Amo, J. L., Pujadas, M., Bigge, K., Kluge, F., Schwarz, A., Daskalakis, N., Walter, D., Zahn, A., Pöschl, U., Bönisch, H., Borrmann, S., Platt, U., Burrows, J. P. (2022). Overview: On the transport and transformation of pollutants in the outflow of major population centres – observational data from the EMeRGe European intensive operational period in summer 2017. *Atmos. Chem. Phys.*, *22*(9), 5877-5924. doi:10.5194/acp-22-5877-2022

Arnold, F., Schneider, J., Gollinger, K., Schlager, H., Schulte, P., Hagen, D. E., Whitefield, P. D., van Velthoven, P. (1997). Observation of upper tropospheric sulfur dioxide- and acetone-pollution: Potential implications for hydroxyl radicaland aerosol formation. *Geophysical Research Letters*, *24*(1), 57-60. doi:10.1029/96gl03693

Brock, C., Hamill, P., Wilson, J., Jonsson, H., & Chan, K. (1995). Particle formation in the upper tropical troposphere: A source of nuclei for the stratospheric aerosol. *Science*, *270*(5242), 1650-1653.

Brühl, C., Lelieveld, J., Crutzen, P. J., Tost, H. (2012). The role of carbonyl sulphide as a source of stratospheric sulphate aerosol and its impact on climate. *Atmos. Chem. Phys.*, *12*(3), 1239-1253. doi:10.5194/acp-12-1239-2012

Carn, S., Krotkov, N., Fioletov, V., Yang, K., Krueger, A., & Tarasick, D. (2008). *Emission, transport and validation of sulfur dioxide in the 2008 Okmok and Kasatochi eruption clouds.* Paper presented at the AGU Fall Meeting Abstracts.

Formatiert: Englisch (Vereinigtes Königreich)

Formatiert: Englisch (Vereinigte Staaten)

Formatiert: Englisch (Vereinigte Staaten)

Clarisse, L., Fromm, M., Ngadi, Y., Emmons, L., Clerbaux, C., Hurtmans, D., & Coheur, P.-F. (2011). Intercontinental transport of anthropogenic sulfur dioxide and other pollutants: An infrared remote sensing case study. *Geophysical Research Letters, 38*(19). doi:https://doi.org/10.1029/2011GL048976

Crutzen, P. J. (2006). Albedo enhancement by stratospheric sulfur injections: a contribution to resolve a policy dilemma? *Climatic change, 77*(3-4), 211.

Cziczo, D. J., Thomson, D. S., & Murphy, D. M. (2001). Ablation, Flux, and Atmospheric Implications of Meteors Inferred from Stratospheric Aerosol. *Science, 291*(5509), 1772-1775. doi:doi:10.1126/science.1057737

de Leeuw, J., Schmidt, A., Witham, C. S., Theys, N., Taylor, I. A., Grainger, R. G., Pope, R. J., Haywood, J., Osborne, M., Kristiansen, N. I. (2021). The 2019 Raikoke volcanic eruption – Part 1: Dispersion model simulations and satellite retrievals of volcanic sulfur dioxide. *Atmos. Chem. Phys., 21*(14), 10851-10879. doi:10.5194/acp-21-10851-2021

Deshler, T. (2008). A review of global stratospheric aerosol: Measurements, importance, life cycle, and local stratospheric aerosol. *Atmospheric Research, 90*(2-4), 223-232.

Deshler, T., Anderson-Sprecher, R., Jäger, H., Barnes, J., Hofmann, D. J., Clemesha, B., Simonich, D., Osborn, M., Grainger, R. G., Godin-Beekmann, S. (2006). Trends in the nonvolcanic component of stratospheric aerosol over the period 1971–2004. *Journal of Geophysical Research: Atmospheres, 111*(D1). doi:https://doi.org/10.1029/2005JD006089

Drewnick, F., Hings, S. S., DeCarlo, P., Jayne, J. T., Gonin, M., Fuhrer, K., Weimer, S., Jimenez, J. L., Demerjian, K. L., Borrmann, S., Worsnop, D. R. (2005). A New Time-of-Flight Aerosol Mass Spectrometer (TOF-AMS)—Instrument Description and First Field Deployment. *Aerosol Science and Technology, 39*(7), 637-658. doi:10.1080/02786820500182040

English, J. M., Toon, O. B., Mills, M. J., & Yu, F. (2011). Microphysical simulations of new particle formation in the upper troposphere and lower stratosphere. *Atmos. Chem. Phys., 11*(17), 9303-9322. doi:10.5194/acp-11-9303-2011

Fiedler, V., Nau, R., Ludmann, S., Arnold, F., Schlager, H., & Stohl, A. (2009). East Asian SO2 pollution plume over Europe – Part 1: Airborne trace gas measurements and source identification by particle dispersion model simulations. *Atmos. Chem. Phys., 9*(14), 4717-4728. doi:10.5194/acp-9-4717-2009

Fischer, H., Wienhold, F. G., Hoor, P., Bujok, O., Schiller, C., Siegmund, P., Ambaum, M., Scheeren, H. A., Lelieveld, J. (2000). Tracer correlations in the northern high latitude lowermost stratosphere: Influence of cross-tropopause mass exchange. *Geophysical Research Letters, 27*(1), 97-100. doi:https://doi.org/10.1029/1999GL010879

Fromm, M., Bevilacqua, R., Servranckx, R., Rosen, J., Thayer, J. P., Herman, J., & Larko, D. (2005). Pyro-cumulonimbus injection of smoke to the stratosphere: Observations and impact of a super blowup in northwestern Canada on 3–4 August 1998. *Journal of Geophysical Research: Atmospheres, 110*(D8). doi:https://doi.org/10.1029/2004JD005350

Fueglistaler, S., Dessler, A., Dunkerton, T., Folkins, I., Fu, Q., & Mote, P. W. (2009). Tropical tropopause layer. *Reviews of Geophysics, 47*(1).

Gottschaldt, K. D., Schlager, H., Baumann, R., Bozem, H., Eyring, V., Hoor, P., Jöckel, P., Jurkat, T., Voigt, C., Zahn, A., Ziereis, H. (2017). Trace gas composition in the Asian summer monsoon anticyclone: a case study based on aircraft observations and model simulations. *Atmos. Chem. Phys., 17*(9), 6091-6111. doi:10.5194/acp-17-6091-2017

Gottschaldt, K. D., Schlager, H., Baumann, R., Cai, D. S., Eyring, V., Graf, P.,Grewe, V., Jöckel, P., Jurkat-Witschas, T., Voigt, C., Zahn, A., Ziereis, H. (2018). Dynamics and composition of the Asian summer monsoon anticyclone. *Atmos. Chem. Phys., 18*(8), 5655-5675. doi:10.5194/acp-18-5655-2018

Hamryszczak, Z. T., Pozzer, A., Obersteiner, F., Bohn, B., Steil, B., Lelieveld, J., & Fischer, H. (2022). Distribution of hydrogen peroxide over Europe during the BLUESKY aircraft campaign. *Atmos. Chem. Phys., 22*(14), 9483-9497. doi:10.5194/acp-22-9483-2022

Hedelt, P., Efremenko, D. S., Loyola, D. G., Spurr, R., & Clarisse, L. (2019). Sulfur dioxide layer height retrieval from Sentinel-5 Precursor/TROPOMI using FP_ILM. *Atmos. Meas. Tech., 12*(10), 5503-5517. doi:10.5194/amt-12-5503-2019

Hegglin, M. I., Boone, C. D., Manney, G. L., & Walker, K. A. (2009). A global view of the extratropical tropopause transition layer from Atmospheric Chemistry Experiment Fourier Transform Spectrometer O3, H2O, and CO. *Journal of Geophysical Research: Atmospheres, 114*(D7). doi:https://doi.org/10.1029/2008JD009984

Hoesly, R. M., Smith, S. J., Feng, L., Klimont, Z., Janssens-Maenhout, G., Pitkanen, T., Seibert, J. J., Vu, L., Andres, R. J., Bolt, R. M., Bond, T. C., Dawidowski, L., Kholod, N., Kurokawa, J. I., Li, M., Liu, L., Lu, Z., Moura, M. C. P., O'Rourke, P. R., Zhang, Q. (2018). Historical (1750–2014) anthropogenic emissions of reactive gases and aerosols from the Community Emissions Data System (CEDS). *Geosci. Model Dev., 11*(1), 369-408. doi:10.5194/gmd-11-369-2018

Hoor, P., Fischer, H., Lange, L., Lelieveld, J., & Brunner, D. (2002). Seasonal variations of a mixing layer in the lowermost stratosphere as identified by the CO-O3 correlation from in situ measurements. *Journal of Geophysical Research: Atmospheres, 107*(D5), ACL 1-1-ACL 1-11. doi:https://doi.org/10.1029/2000JD000289

Junge, C. E., Chagnon, C. W., & Manson, J. E. (1961). Stratospheric aerosols. *Journal of Atmospheric Sciences, 18*(1), 81-108.

Jurkat, T., Kaufmann, S., Voigt, C., Schäuble, D., Jeßberger, P., Ziereis, H. (2016). The airborne mass spectrometer AIMS – Part 2: Measurements of trace gases with stratospheric or tropospheric origin in the UTLS. *Atmos. Meas. Tech., 9*(4), 1907-1923. doi:10.5194/amt-9-1907-2016

Feldfunktion geändert
Formatiert: Englisch (Vereinigte Staaten)
Formatiert: Englisch (Vereinigte Staaten)
Feldfunktion geändert
Formatiert: Englisch (Vereinigte Staaten)
Formatiert: Englisch (Vereinigte Staaten)
Formatiert: Englisch (Vereinigte Staaten)
Feldfunktion geändert
Formatiert: Englisch (Vereinigte Staaten)
Formatiert: Englisch (Vereinigte Staaten)
Feldfunktion geändert
Formatiert: Englisch (Vereinigte Staaten)
Formatiert: Englisch (Vereinigte Staaten)
Formatiert: Englisch (Vereinigte Staaten)
Formatiert: Englisch (Vereinigte Staaten)
Feldfunktion geändert
Formatiert: Englisch (Vereinigte Staaten)
Formatiert: Englisch (Vereinigte Staaten)
Formatiert: Englisch (Vereinigte Staaten)
Feldfunktion geändert
Formatiert: Englisch (Vereinigte Staaten)
Formatiert: Englisch (Vereinigte Staaten)
Formatiert: Englisch (Vereinigte Staaten)

Jurkat, T., Voigt, C., Arnold, F., Schlager, H., Aufmhoff, H., Schmale, J., Schneider, J., Lichtenstern, M., Dörnbrack, A. (2010). Airborne stratospheric ITCIMS measurements of SO2, HCl, and HNO3in the aged plume of volcano Kasatochi. *Journal of Geophysical Research, 115*. doi:10.1029/2010jd013890

Jurkat, T., Voigt, C., Arnold, F., Schlager, H., Kleffmann, J., Aufmhoff, H., Schäuble, D., Schaefer, M., Schumann, U. (2011). Measurements of HONO, NO, NOyand SO2in aircraft exhaust plumes at cruise. *Geophysical Research Letters, 38*(10), n/a-n/a. doi:10.1029/2011gl046884

Jurkat, T., Voigt, C., Kaufmann, S., Zahn, A., Sprenger, M., Hoor, P., Bozem, H., Müller, S., Dörnbrack, A., Schlager, H., Bönisch, H., Engel, A. (2014). A quantitative analysis of stratospheric HCl, HNO3, and O3in the tropopause region near the subtropical jet. *Geophysical Research Letters, 41*(9), 3315-3321. doi:10.1002/2013gl059159

Kaufmann, S., Voigt, C., Heller, R., Jurkat-Witschas, T., Krämer, M., Rolf, C., Zöger, M., Giez, A., Buchholz, B., Ebert, V., Thornberry, T., Schumann, U. (2018). Intercomparison of midlatitude tropospheric and lower-stratospheric water vapor measurements and comparison to ECMWF humidity data. *Atmos. Chem. Phys., 18*(22), 16729-16745. doi:10.5194/acp-18-16729-2018

Kirkby, J., Curtius, J., Almeida, J., Schobesberger, S., Kürten, A., Ortega, I. K., Kupiainen-Määttä, O., Praplan, A. P., Adamov, A., Amorim, A., Bianchi, F., Breitenlechner, M., David, A., Dommen, J., Donahue, N. M., Downard, A., Dunne, E., Duplissy, J., Ehrhart, S., Flagan, R, & Dunne, E., Duplissy, J., Ehrhart, S., Franchin, A., Gagné, S., Ickes, L., Kürten, A., Kupc, A., Metzger, A., Riccobono, F., Rondo, L., Schobesberger, S., Tsagkogeorgas, G., Wimmer, D., Amorim, A., Bianchi, F., Breitenlechner, M., David, A., Dommen, J., Downard, A., Ehn, M., Flagan, R. C., Haider, S., Hansel, A., Hauser, D., Jud, W., Junninen, H., Kreissl, F., Kvashin, A., Laaksonen, A., Lehtipalo, K., Lima, J., Lovejoy, E. R., Makhmutov, V., Mathot, S., Mikkilä, J., Minginette, P., Mogo, S., Nieminen, T., Onnela, A., Pereira, P., Petäjä, T., Schnitzhofer, R., Seinfeld, J. H., Sipilä, M., Stozhkov, Y., Stratmann, F., Tomé, A., Vanhanen, J., Viisanen, Y., Vrtala, A., Wagner, P. E., Walther, H., Weingartner, E., Wex, H., Winkler, P. M., Carslaw, K. S., Worsnop, D. R., Baltensperger, U., Kulmala, M. (2011). Role of sulphuric acid, ammonia and galactic cosmic rays in atmospheric aerosol nucleation. *Nature, 476*(7361), 429-433. doi:10.1038/nature10343

Klausner, T., Mertens, M., Huntrieser, H., Galkowski, M., Kuhlmann, G., Baumann, R., Fiehn, A., Jöckel, P., Pühl, M., Roiger, A. (2020). Urban greenhouse gas emissions from the Berlin area: A case study using airborne CO2 and CH4 in situ observations in summer 2018. *Elementa: Science of the Anthropocene, 8*. doi:10.1525/elementa.411

Kloss, C., Berthet, G., Sellitto, P., Ploeger, F., Taha, G., Tidiga, M., Eremenko, M., Bossolasco, A., Jégou, F., Renard, J.-B., Legras, B. (2021). Stratospheric aerosol layer perturbation caused by the 2019 Raikoke and Ulawun eruptions and their radiative forcing. *Atmospheric Chemistry and Physics, 21*(1), 535-560. doi:10.5194/acp-21-535-2021

Kremser, S., Thomason, L. W., von Hobe, M., Hermann, M., Deshler, T., Anderson-Sprecher, R., Jäger, H., Barnes, J., Hofmann, D. J., Clemesha, B., Simonich, D., Osborn, M., Grainger, R. G., Godin-Beekmann, S., Timmreck, C., Toohey, M., Stenke, A., Schwarz, J. P., Weigel, R. (2016). Stratospheric aerosol—Observations, processes, and impact on climate. *J Reviews of Geophysics, 54*(2), 278-335.

Krippner, J. B., and Venzke, E., eds. (2020). Global Volcanism Program, 2020. Report on Taal (Philippines) *Global Volcanism Program, 45*. doi:https://doi.org/10.5479/si.GVP.BGVN202006-273070

Krüger, O. O., Holanda, B. A., Chowdhury, S., Pozzer, A., Walter, D., Pöhlker, C., Andrés Hernández, M. D., Burrows, J. P., Voigt, C., Lelieveld, J., Quaas, J., Pöschl, U., Pöhlker, M. L. (2022). Black carbon aerosol reductions during COVID-19 confinement quantified by aircraft measurements over Europe. *Atmos. Chem. Phys., 22*(13), 8683-8699. doi:10.5194/acp-22-8683-2022

Lee, C., Martin, R. V., van Donkelaar, A., Lee, H., Dickerson, R. R., Hains, J. C., Krotkov, N., Richter, A., Vinnikov, K., Schwab, J. J. (2011). SO2 emissions and lifetimes: Estimates from inverse modeling using in situ and global, space-based (SCIAMACHY and OMI) observations. *Journal of Geophysical Research: Atmospheres, 116*(D6). doi:https://doi.org/10.1029/2010JD014758

Lee, D. S., Fahey, D.W., Skowron, A., Allen, M.R., Burkhardt, U., Chen, Q., Doherty, S.J., Freeman, S., Forster, P.M., Fuglestvedt, J (2021). The contribution of global aviation to anthropogenic climate forcing for 2000 to 2018. *J Atmospheric environment, 244*, 117834.

Lee, D. S., Pitari, G., Grewe, V., Gierens, K., Penner, J. E., Petzold, A., Prather, M.J., Schumann, U., Bais, A., Berntsen, T. (2010). Transport impacts on atmosphere and climate: Aviation. *J Atmospheric environment, 44*(37), 4678-4734.

Lelieveld, J. (1993). Multi-phase processes in the atmospheric sulfur cycle. In *Interactions of C, N, P and S biogeochemical cycles and global change* (pp. 305-331): Springer.

Liu, F., Xing, C., Li, J., Wang, B., Chai, J., Gao, C., Huang, G., Liu, J., Chen, D. (2020). Could the Recent Taal Volcano Eruption Trigger an El Niño and Lead to Eurasian Warming? *Advances in Atmospheric Sciences, 37*(7), 663-670. doi:10.1007/s00376-020-2041-z

Marsing, A. (2021). *Chlorine Partitioning in the Lowermost Arctic Stratosphere During Winter-an Aircraft in Situ Measurement Perspective.* (PhD diss.). Johannes Gutenberg-Universität Mainz,

Marsing, A., Jurkat-Witschas, T., Grooß, J. U., Kaufmann, S., Heller, R., Engel, A., Hoor, P., Krause, J., Voigt, C. (2019). Chlorine partitioning in the lowermost Arctic vortex during the cold winter 2015/2016. *Atmos. Chem. Phys., 19*(16), 10757-10772. doi:10.5194/acp-19-10757-2019

Martinsson, B. G., Brenninkmeijer, C. A. M., Carn, S. A., Hermann, M., Heue, K.-P., van Velthoven, P. F. J., & Zahn, A. (2009). Influence of the 2008 Kasatochi volcanic eruption on sulfurous and carbonaceous aerosol constituents in the lower stratosphere. *Geophysical Research Letters, 36*(12). doi:https://doi.org/10.1029/2009GL038735

Formatiert: Englisch (Vereinigte Staaten)

Formatiert: Englisch (Vereinigte Staaten)

Formatiert: Englisch (Vereinigte Staaten)

Formatiert: Englisch (Vereinigte Staaten)

Feldfunktion geändert

Formatiert: Englisch (Vereinigte Staaten)

Formatiert: Englisch (Vereinigte Staaten)

Formatiert: Englisch (Vereinigte Staaten)

Feldfunktion geändert

Formatiert: Englisch (Vereinigte Staaten)

Formatiert: Englisch (Vereinigte Staaten)

Formatiert: Englisch (Vereinigte Staaten)

Feldfunktion geändert

Formatiert: Englisch (Vereinigte Staaten)

Formatiert: Englisch (Vereinigte Staaten)

Martinsson, B. G., Nguyen, H. N., Brenninkmeijer, C. A. M., Zahn, A., Heintzenberg, J., Hermann, M., & van Velthoven, P. F. J. (2005). Characteristics and origin of lowermost stratospheric aerosol at northern midlatitudes under volcanically quiescent conditions based on CARIBIC observations. *Journal of Geophysical Research: Atmospheres*, *110*(D12). doi:https://doi.org/10.1029/2004JD005644

Martinsson, B. G., Papaspiropoulos, G., Heintzenberg, J., & Hermann, M. J. G. r. l. (2001). Fine mode participate sulphur in the tropopause region measured from intercontinental flights (CARIBIC). *Geophysical Research Letters*, *28*(7), 1175-1178.

McCormick, M. P., Thomason, L. W., & Trepte, C. R. (1995). Atmospheric effects of the Mt Pinatubo eruption. *Nature*, *373*(6513), 399-404.

Molleker, S., Helleis, F., Klimach, T., Appel, O., Clemen, H. C., Dragoneas, A., Gurk, C., Hünig, A., Köllner, F., Rubach, F., Schulz, C., Schneider, J., Borrmann, S. (2020). Application of an O-ring pinch device as a constant-pressure inlet (CPI) for airborne sampling. *Atmos. Meas. Tech.*, *13*(7), 3651-3660. doi:10.5194/amt-13-3651-2020

Morgan, W. T., Allan, J. D., Bower, K. N., Capes, G., Crosier, J., Williams, P. I., & Coe, H. (2009). Vertical distribution of sub-micron aerosol chemical composition from North-Western Europe and the North-East Atlantic. *Atmos. Chem. Phys.*, *9*(15), 5389-5401. doi:10.5194/acp-9-5389-2009

Murphy, D., Froyd, K., Schwarz, J., & Wilson, J. (2014). Observations of the chemical composition of stratospheric aerosol particles. *Quarterly Journal of the Royal Meteorological Society*, *140*(681), 1269-1278.

Nussbaumer, C. M., Pozzer, A., Tadic, I., Röder, L., Obersteiner, F., Harder, H., Lelieveld, J., Fischer, H. (2022). Tropospheric ozone production and chemical regime analysis during the COVID-19 lockdown over Europe. *Atmos. Chem. Phys.*, *22*(9), 6151-6165. doi:10.5194/acp-22-6151-2022

Osborne, M. J., de Leeuw, J., Witham, C., Schmidt, A., Beckett, F., Kristiansen, N., Buxmann, J., Saint, C., Welton, E. J., Fochesatto, J., Gomes, A. R., Bundke, U., Petzold, A., Marenco, F., Haywood, J. (2022). The 2019 Raikoke volcanic eruption – Part 2: Particle-phase dispersion and concurrent wildfire smoke emissions. *Atmos. Chem. Phys.*, *22*(5), 2975-2997. doi:10.5194/acp-22-2975-2022

Pan, L. L., Randel, W. J., Gary, B. L., Mahoney, M. J., & Hintsa, E. J. (2004). Definitions and sharpness of the extratropical tropopause: A trace gas perspective. *Journal of Geophysical Research: Atmospheres*, *109*(D23). doi:https://doi.org/10.1029/2004JD004982

Peterson, D. A., Campbell, J. R., Hyer, E. J., Fromm, M. D., Kablick, G. P., Cossuth, J. H., & DeLand, M. T. (2018). Wildfire-driven thunderstorms cause a volcano-like stratospheric injection of smoke. *npj Climate and Atmospheric Science*, *1*(1), 30. doi:10.1038/s41612-018-0039-3

Ploeger, F., Konopka, P., Walker, K., & Riese, M. (2017). Quantifying pollution transport from the Asian monsoon anticyclone into the lower stratosphere. *Atmos. Chem. Phys.*, *17*(11), 7055-7066. doi:10.5194/acp-17-7055-2017

Reifenberg, S. F., Martin, A., Kohl, M., Hamryszczak, Z., Tadic, I., Röder, L., Crowley, D. J., Fischer, H., Kaiser, K., Schneider, J., Dörich, R., Crowley, J. N., Tomsche, L., Marsing, A., Voigt, C., Zahn, A., Pöhlker, C., Holanda, B., Krüger, O. O., Pöschl, U., Pöhlker, M., Jöckel, P., Dorf, M., Schumann, U., Williams, J., Curtius, J., Harder, H., Schlager, H., Lelieveld, J., Pozzer, A. (2021). Impact of reduced emissions on direct and indirect aerosol radiative forcing during COVID–19 lockdown in Europe. *Atmos. Chem. Phys. Discuss.*, *2021*, 1-23. doi:10.5194/acp-2021-1005

Rolph, G., Stein, A., & Stunder, B. (2017). Real-time Environmental Applications and Display sYstem: READY. *Environmental Modelling & Software*, *95*, 210-228. doi:https://doi.org/10.1016/j.envsoft.2017.06.025

Schäfer, S., Lawrence, M., Stelzer, H., Born, W., Low, S., Aaheim, A., Adriázola, P., Betz, G., Boucher, O., Carius, A., Devine-Right, P., Gullberg, A. T., Haszeldine, S., Haywood, J., Houghton, K., Ibarrola, R., Irvine, P., Kristjansson, J.-E., Lenton, T., Link, J. S. A., Maas, A., Meyer, L., Muri, H., Oschlies, A., Proelß, A., Rayner, T., Rickels, W., Ruthner, L., Scheffran, J., Schmidt, H., Schulz, M., Scott, V., Shackley, S., Tänzler, D., Watson, M., Vaughan, N. (2015). The European transdisciplinary assessment of climate engineering (EuTRACE): Removing greenhouse gases from the atmosphere and reflecting sunlight away from Earth. *Funded by the European Union's Seventh Framework Programme under Grant Agreement 306993.* Retrieved from www.eutrace.org

Schiller, C. L., Bozem, H., Gurk, C., Parchatka, U., Königstedt, R., Harris, G. W., Lelieveld, J., Fischer, H. (2008). Applications of quantum cascade lasers for sensitive trace gas measurements of CO, CH4, N2O and HCHO. *Applied Physics B*, *92*(3), 419-430. doi:10.1007/s00340-008-3125-0

Schmale, J., Schneider, J., Jurkat, T., Voigt, C., Kalesse, H., Rautenhaus, M., Lichtenstern, M., Schlager, H., Ancellet, G., Arnold, F., Gerding, M., Mattis, I., Wendisch, M., Borrmann, S. (2010). Aerosol layers from the 2008 eruptions of Mount Okmok and Mount Kasatochi: In situ upper troposphere and lower stratosphere measurements of sulfate and organics over Europe. *Journal of Geophysical Research*, *115*. doi:10.1029/2009jd013628

Schneider, J., Hings, S. S., Hock, N. B., Weimer, S., Borrmann, S., Fiebig, M., Petzold, A., Busen, R., Kärcher, B. (2006). Aircraft-based operation of an aerosol mass spectrometer: Measurements of tropospheric aerosol composition. *Journal of Aerosol Science*, *37*(7), 839-857. doi:https://doi.org/10.1016/j.jaerosci.2005.07.002

Schneider, J., Weigel, R., Klimach, T., Dragoneas, A., Appel, O., Hünig, A., Molleker, S., Köllner, F., Clemen, H. C., Eppers, O., Hoppe, P., Hoor, P., Mahnke, C., Krämer, M., Rolf, C., Grooß, J. U., Zahn, A., Obersteiner, F., Ravegnani, F., Ulanovsky, A., Schlager, H., Scheibe, M., Diskin, G. S., DiGangi, J. P., Nowak, J. B., Zöger, M., Borrmann, S. (2021). Aircraft-based observation of

Formatiert: Englisch (Vereinigte Staaten)
Formatiert: Englisch (Vereinigte Staaten)
Feldfunktion geändert
Formatiert: Englisch (Vereinigte Staaten)
Feldfunktion geändert
Formatiert: Englisch (Vereinigte Staaten)
Formatiert: Englisch (Vereinigte Staaten)
Formatiert: Englisch (Vereinigte Staaten)
Feldfunktion geändert
Formatiert: Englisch (Vereinigte Staaten)
Formatiert: Englisch (Vereinigte Staaten)
Formatiert: Englisch (Vereinigte Staaten)
Feldfunktion geändert
Formatiert: Englisch (Vereinigte Staaten)
Formatiert: Englisch (Vereinigte Staaten)

meteoric material in lower-stratospheric aerosol particles between 15 and 68° N. *Atmos. Chem. Phys., 21*(2), 989-1013. doi:10.5194/acp-21-989-2021

Schulte, P., & Schlager, H. (1996). In-flight measurements of cruise altitude nitric oxide emission indices of commercial jet aircraft. *Geophysical Research Letters, 23*(2), 165-168. doi:https://doi.org/10.1029/95GL03691

Schulz, C., Schneider, J., Amorim Holanda, B., Appel, O., Costa, A., de Sá, S. S., Dreiling, V., Fütterer, D., Jurkat-Witschas, T., Klimach, T., Knote, C., Krämer, M., Martin, S. T., Mertes, S., Pöhlker, M. L., Sauer, D., Voigt, C., Walser, A., Weinzierl, B., Ziereis, H., Zöger, M., Andreae, M. O., Artaxo, P., Machado, L. A. T., Pöschl, U., Wendisch, M., Borrmann, S. (2018). Aircraft-based observations of isoprene-epoxydiol-derived secondary organic aerosol (IEPOX-SOA) in the tropical upper troposphere over the Amazon region. *Atmos. Chem. Phys., 18*(20), 14979-15001. doi:10.5194/acp-18-14979-2018

Schumann, U., Bugliaro, L., Dörnbrack, A., Baumann, R., Voigt, C. (2021). Aviation Contrail Cirrus and Radiative Forcing Over Europe During 6 Months of COVID-19. *Geophysical Research Letters, 48*(8), e2021GL092771. doi:https://doi.org/10.1029/2021GL092771

Schumann, U., Poll, I., Teoh, R., Koelle, R., Spinielli, E., Molloy, J., Koudis, G. S., Baumann, R., Bugliaro, L., Stettler, M., Voigt, C. (2021). Air traffic and contrail changes over Europe during COVID-19: a model study. *Atmos. Chem. Phys., 21*(10), 7429-7450. doi:10.5194/acp-21-7429-2021

Seinfeld, J. H., & Pandis, S. N. (2006). *Atmospheric chemistry and physics: from air pollution to climate change*: John Wiley & Sons.

Sheng, J.-X., Weisenstein, D. K., Luo, B.-P., Rozanov, E., Stenke, A., Anet, J., Bingemer, H., Peter, T. (2015). Global atmospheric sulfur budget under volcanically quiescent conditions: Aerosol-chemistry-climate model predictions and validation. *Journal of Geophysical Research: Atmospheres, 120*(1), 256-276. doi:https://doi.org/10.1002/2014JD021985

Speidel, M., Nau, R., Arnold, F., Schlager, H., & Stohl, A. (2007). Sulfur dioxide measurements in the lower, middle and upper troposphere: Deployment of an aircraft-based chemical ionization mass spectrometer with permanent in-flight calibration. *Atmospheric Environment, 41*(11), 2427-2437. doi:10.1016/j.atmosenv.2006.07.047

Stein, A. F., Draxler, R. R., Rolph, G. D., Stunder, B. J., Cohen, M. D., Ngan, F. (2015). NOAA's HYSPLIT atmospheric transport and dispersion modeling system. *Bulletin of the American Meteorological Society, 96(12)*, 2059-2077.

Stockwell, W. R., & Calvert, J. G. (1983). The mechanism of the HO-SO_2 reaction. *Atmospheric Environment (1967), 17*(11), 2231-2235. doi:https://doi.org/10.1016/0004-6981(83)90220-2

Thouret, V., Cammas, J. P., Sauvage, B., Athier, G., Zbinden, R., Nédélec, P., Simon, P., Karcher, F. (2006). Tropopause referenced ozone climatology and inter-annual variability (1994–2003) from the MOZAIC programme. *Atmos. Chem. Phys., 6*(4), 1033-1051. doi:10.5194/acp-6-1033-2006

Tomsche, L., Pozzer, A., Ojha, N., Parchatka, U., Lelieveld, J., & Fischer, H. (2019). Upper tropospheric CH_4 and CO affected by the South Asian summer monsoon during the Oxidation Mechanism Observations mission. *Atmos. Chem. Phys., 19*(3), 1915-1939. doi:10.5194/acp-19-1915-2019

van Heerwaarden, C. C., Mol, W. B., Veerman, M. A., Benedict, I., Heusinkveld, B. G., Knap, W. H., Kazadzis, S., Kouremeti, N., Fiedler, S. (2021). Record high solar irradiance in Western Europe during first COVID-19 lockdown largely due to unusual weather. *Communications Earth & Environment, 2*(1), 37. doi:10.1038/s43247-021-00110-0

Vogel, B., Günther, G., Müller, R., Grooß, J.-U., Afchine, A., Bozem, H., Hoor, P., Krämer, M., Müller, S., Riese, M., Rolf, C., Spelten, N., Stiller, G. P., Ungermann, J., Zahn, A. (2016). Long-range transport pathways of tropospheric source gases originating in Asia into the northern lower stratosphere during the Asian monsoon season 2012. *Atmospheric Chemistry and Physics, 16*(23), 15301-15325. doi:10.5194/acp-16-15301-2016

Vogel, B., Günther, G., Müller, R., Grooß, J. U., Hoor, P., Krämer, M., Müller, S., Zahn, A., Riese, M. (2014). Fast transport from Southeast Asia boundary layer sources to northern Europe: rapid uplift in typhoons and eastward eddy shedding of the Asian monsoon anticyclone. *Atmospheric Chemistry and Physics, 14*(23), 12745-12762. doi:10.5194/acp-14-12745-2014

Vogel, B., Müller, R., Günther, G., Spang, R., Hanumanthu, S., Li, D., Riese, M., Stiller, G. P. (2019). Lagrangian simulations of the transport of young air masses to the top of the Asian monsoon anticyclone and into the tropical pipe. *Atmospheric Chemistry and Physics, 19*(9), 6007-6034. doi:10.5194/acp-19-6007-2019

Voigt, C., Jessberger, P., Jurkat, T., Kaufmann, S., Baumann, R., Schlager, H., Bobrowski, N., Giuffrida, G., Salerno, G. (2014). Evolution of CO_2, SO_2, HCl, and HNO_3in the volcanic plumes from Etna. *Geophysical Research Letters, 41*(6), 2196-2203. doi:10.1002/2013gl058974

Voigt, C., Lelieveld, J., Schlager, H., Schneider, J., Curtius, J., Meerkötter, R., Sauer, D., Bugliaro, L., Bohn, B., Crowley, J. N., Erbertseder, T., Groß, S., Hahn, V., Li, Q., Mertens, M., Pöhlker, M. L., Pozzer, A., Schumann, U., Tomsche, L., Williams, J., Zahn, A., Andreae, M., Borrmann, S., Bräuer, T., Dörich, R., Dörnbrack, A., Edtbauer, A., Ernle, L., Fischer, H., Giez, A., Granzin, M., Grewe, V., Harder, H., Heinritzi, M., Holanda, B. A., Jöckel, P., Kaiser, K., Krüger, O. O., Lucke, J., Marsing, A., Martin, A., Matthes, S., Pöhlker, C., Pöschl, U., Reifenberg, S., Ringsdorf, A., Scheibe, M., Tadic, I., Zauner-Wieczorek, M., Henke, R., Rapp, M. (2022). Cleaner skies during the COVID-19 lockdown. *Bulletin of the American Meteorological Society*. doi:10.1175/bams-d-21-0012.1

Feldfunktion geändert
Formatiert: Englisch (Vereinigte Staaten)
Formatiert: Englisch (Vereinigte Staaten)
Formatiert: Englisch (Vereinigte Staaten)
Feldfunktion geändert
Formatiert: Englisch (Vereinigte Staaten)
Formatiert: Englisch (Vereinigte Staaten)
Formatiert: Englisch (Vereinigte Staaten)
Feldfunktion geändert
Formatiert: Englisch (Vereinigte Staaten)
Formatiert: Englisch (Vereinigte Staaten)
Feldfunktion geändert
Formatiert: Englisch (Vereinigte Staaten)
Formatiert: Englisch (Vereinigte Staaten)
Formatiert: Englisch (Vereinigte Staaten)
Formatiert: Englisch (Vereinigte Staaten)
Formatiert: Englisch (Vereinigte Staaten)
Formatiert: Englisch (Vereinigte Staaten)

Voigt, C., Schumann, U., Jurkat, T., Schäuble, D., Schlager, H., Petzold, A., Gayet, J. F., Krämer, M., Schneider, J., Borrmann, S., Schmale, J., Jessberger, P., Hamburger, T., Lichtenstern, M., Scheibe, M., Gourbeyre, C., Meyer, J., Kübbeler, M., Frey, W., Kalesse, H., Butler, T., Lawrence, M. G., Holzäpfel, F., Arnold, F., Wendisch, M., Döpelheuer, A., Gottschaldt, K., Baumann, R., Zöger, M., Sölch, I., Rautenhaus, M., Dörnbrack, A. (2010). In-situ observations of young contrails – overview and selected results from the CONCERT campaign. *Atmos. Chem. Phys., 10*(18), 9039-9056. doi:10.5194/acp-10-9039-2010

von Hobe, M., Ploeger, F., Konopka, P., Kloss, C., Ulanowski, A., Yushkov, V., Ravegnani, F., Volk, C. M., Pan, L. L., .Honomichl, S. B., Tilmes, S., Kinnison, D. E., Garcia, R. R., Wright, J. S. (2021). Upward transport into and within the Asian monsoon anticyclone as inferred from StratoClim trace gas observations. *Atmos. Chem. Phys., 21*(2), 1267-1285. doi:10.5194/acp-21-1267-2021

Williamson, C. J., Kupc, A., Rollins, A., Kazil, J., Froyd, K. D., Ray, E. A., Murphy, D. M., Schill, G. P., Peischl, J., Thompson, C., Bourgeois, I., Ryerson, T. B., Diskin, G. S., DiGangi, J. P., Blake, D. R., Bui, T. P. V., Dollner, M., Weinzierl, B., Brock, C. A. (2021). Large hemispheric difference in nucleation mode aerosol concentrations in the lowermost stratosphere at mid- and high latitudes. *Atmos. Chem. Phys., 21*(11), 9065-9088. doi:10.5194/acp-21-9065-2021

Zahn, A., Weppner, J., Widmann, H., Schlote-Holubek, K., Burger, B., Kühner, T., Franke, H. (2012). A fast and precise chemiluminescence ozone detector for eddy flux and airborne application. *Atmos. Meas. Tech., 5*(2), 363-375. doi:10.5194/amt-5-363-2012

Ziereis, H., Schlager, H., Schulte, P., van Velthoven, P. F. J., & Slemr, F. (2000). Distributions of NO, NO x , and NO y in the upper troposphere and lower stratosphere between 28° and 61°N during POLINAT 2. *Journal of Geophysical Research: Atmospheres, 105*(D3), 3653-3664. doi:https://doi.org/10.1029/1999JD900870

Formatiert: Englisch (Vereinigte Staaten)

Formatiert: Englisch (Vereinigte Staaten)

Formatiert: Englisch (Vereinigte Staaten)